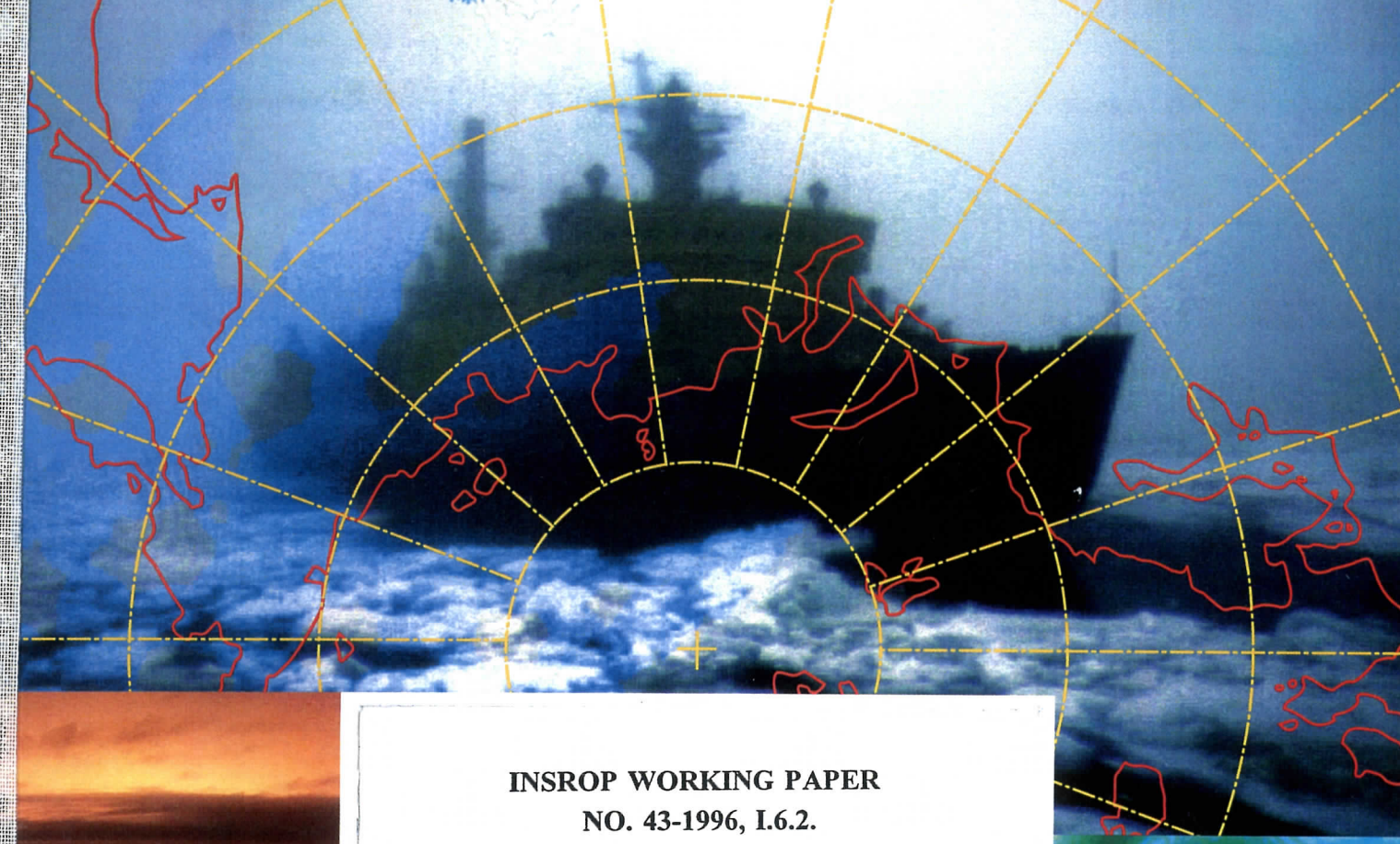

INSROP WORKING PAPER
NO. 43-1996, I.6.2.

Behaviour of Ice Floe in Restricted Waters

Hajime Yamaguchi

INSROP International Northern Sea Route Programme

Central Marine Research & Design Institute, Russia

The Fridtjof Nansen Institute, Norway

Ship and Ocean Foundation, Japan

International Northern Sea Route Programme (INSROP)

Central Marine Research & Design Institute, Russia

The Fridtjof Nansen Institute, Norway

Ship & Ocean Foundation, Japan

INSROP WORKING PAPER NO. 43-1996

Sub-programme I: Natural Conditions and Ice Navigation

Project I.6.2: Behaviour of Ice Floe in Restricted Waters.

By:
Dr. Hajime Yamaguchi (Supervisor)

Address:
Department of Naval Architecture and Ocean Engineering
Graduate School of Engineering
University of Tokyo
7-3-1, Hongo, Bunkyo-ku
Tokyo 113
JAPAN

Date: 9 April 1996.

Reviewed by:
Professor Wiliam Sackinger, OBELISK Hydrocarbons (Alaska) Ltd.,
Fairbanks, Alaska, USA.

What is an INSROP Working Paper and how to handle it:

FOREWORD - INSROP WORKING PAPER

INSROP is a five-year multidisciplinary and multilateral research programme, the main phase of which commenced in June 1993. The three principal cooperating partners are **Central Marine Research & Design Institute (CNIIMF)**, St. Petersburg, Russia; **Ship and Ocean Foundation (SOF)**, Tokyo, Japan; and **Fridtjof Nansen Institute (FNI)**, Lysaker, Norway. The INSROP Secretariat is shared between CNIIMF and FNI and is located at FNI.

INSROP is split into four main projects: 1) Natural Conditions and Ice Navigation; 2) Environmental Factors; 3) Trade and Commercial Shipping Aspects of the NSR; and 4) Political, Legal and Strategic Factors. The aim of INSROP is to build up a knowledge base adequate to provide a foundation for long-term planning and decision-making by state agencies as well as private companies etc., for purposes of promoting rational decisionmaking concerning the use of the Northern Sea Route for transit and regional development.

INSROP is a direct result of the normalization of the international situation and the Murmansk initiatives of the former Soviet Union in 1987, when the readiness of the USSR to open the NSR for international shipping was officially declared. The Murmansk Initiatives enabled the continuation, expansion and intensification of traditional collaboration between the states in the Arctic, including safety and efficincy of shipping. Russia, beeing the successor state to the USSR, supports the Murmansk Initiatives. The initiatives stimulated contact and cooperation between CNIIMF and FNI in 1988 and resulted in a pilot study of the NSR in 1991. In 1992 SOF entered INSROP as a third partner on an equal basis with CNIIMF and FNI.

The complete series of publications may be obtained from the Fridtjof Nansen Institute.

SPONSORS FOR INSROP

- Nippon Foundation/Ship & Ocean Foundation, Japan
- The government of the Russian Federation
- The Norwegian Research Council
- The Norwegian Ministry of Foreign Affairs
- The Norwegian Ministry of Industry and Energy
- The Norwegian Ministry of the Environment
- State Industry and Regional Development Fund, Norway
- Norsk Hydro
- Norwegian Federation of Shipowners
- Fridtjof Nansen Institute
- Kværner a.s.

PROFESSIONAL ORGANISATIONS PERMANENTLY ATTACHED TO INSROP

- Ship & Ocean Foundation, Japan
- Central Marine Research & Design Institute, Russia
- Fridtjof Nansen Institute, Norway
- National Institute of Polar Research, Japan
- Ship Research Institute, Japan
- Murmansk Shipping Company, Russia
- Northern Sea Route Administration, Russia
- Arctic & Antarctic Research Institute, Russia
- ARTEC, Norway
- Norwegian Polar Research Institute
- Norwegian School of Economics and Business Administration
- SINTEF NHL (Foundation for Scientific and Industrial Research - Norwegian Hydrotechnical Laboratory), Norway.

PROGRAMME COORDINATORS

- **Yuri Ivanov, CNIIMF**
  Kavalergardskaya Str.6
  St. Petersburg 193015, Russia
  Tel: 7 812 271 5633
  Fax: 7 812 274 3864
  Telex: 12 14 58 CNIMF SU
- **Willy Østreng, FNI**
  P.O. Box 326
  N-1324 Lysaker, Norway
  Tel: 47 67 11 19 00
  Fax: 47 67 11 19 10
  E-mail: sentralbord@fni.wpoffice.telemax.no
- **Masaru Sakuma, SOF**
  Senpaku Shinko Building
  15-16 Toranomon 1-chome
  Minato-ku, Tokyo 105, Japan
  Tel: 81 3 3502 2371
  Fax: 81 3 3502 2033
  Telex: J 23704

Project I.6.2 : Behavior of ice floe in restricted waters

by

Dr. Hajime Yamaguchi (Supervisor)
Department of Naval Architecture and Ocean Engineering
Graduate School of Engineering
University of Tokyo
7-3-1, Hongo, Bunkyo-ku, Tokyo 113 JAPAN
Phone: #81-3-3812-2111 ext.6536
Fax: #81-3-3815-8360
E-mail: *yama@fluidlab.naoe.t.u-tokyo.ac.jp*

March 1996

Table of Contents

PART I : Model Development of Distributed Mass / Discrete Floe Model

Abstract 1

Nomenclatures 1

1. Introduction 2
2. Ice Model 3
3. Equations of Bunch Motion 5
4. Ice Interaction Force 6
   - 4.1 Axial ice interaction 6
   - 4.2 Lateral expansion of floes 7
5. Movement and Deformation of Bunch 10
6. Redistribution of Pack Ice 11
7. Ocean Flow 13

Summary and Conclusions 14

References 15

PART II : Model Verification

- Comparison to Circulation Water Channel Experiments and Sea Ice Motion in the Southern Part of the Okhotsk -

Abstract 16

1. Introduction 16
2. Drift Tests of Physical Model Floes 17
   - 2.1 Experimental set-up 17
   - 2.2 Wind and current distribution 18
3. Experimental Results 19
   - 3.1 Free drift of physical model floes 19
   - 3.2 Drift of physical model floes around no water stop structure 20
   - 3.3 Drift of physical model floes around water stop structure 20
4. Motion Simulations of the Physical Model Floes 21
   - 4.1 Computation parameters 21
   - 4.2 Drift of physical model floes around no water stop structure 22
   - 4.3 Drift of physical model floes around water stop structure 23
5. Simulation of Sea Ice Motion in the Southern Part of the Sea of Okhotsk 23
   - 5.1 Computation conditions 23
   - 5.2 Numerical result 24
6. Summary and Conclusions 24

Acknowledgment 24

PART I : Model Development of Distributed Mass / Discrete Floe Model

Abstract

A new model, named "Distributed Mass / Discrete Floe model", is proposed for practical computations of mesoscale pack ice rheology. This model possesses the advantages of both the continuum and the discrete element ones: it can express the discrete nature of pack ice which is difficult for a continuum model to treat, and can realize much shorter computation time than a discrete element model. The pack ice is divided into ice floe bunches in which the floes, assumed to be distributed uniformly, are modeled as inelastic circular disks and/or rectangles floating on the water. The ice interaction forces are formulated from the relation between the impulse on the bunch and the variation of the bunch momentum. The ocean flow is calculated by a multi-layer model simultaneously with the ice floe movement.

Nomenclatures

A_i	Total surface area of floes in a bunch
bc_x	Center position of floe bunch in x-direction
bc_y	Center position of floe bunch in y-direction
bl_x	Ice bunch length in x-direction
bl_y	Ice bunch length in y-direction
C_a	Friction coefficient between air and ice
C_d	Friction coefficient between air and water
C_w	Friction coefficient between water and ice
C_i	Ice concentration (ratio of ice area to bunch area)
dl_{ic}	Diameter of the circular disk floe
dl_{ix}	Rectangle floe size in x-direction
dl_{iy}	Rectangle floe size in y-direction
E_{ij}	Eddy viscosity
f	Coriolis parameter, $2\omega \sin\phi$
g	Acceleration of gravity
h_i	Ice thickness
$\bar{k}$	Unit vector in depth direction
M_i	Ice bunch mass

N_{ix}	Number of floes in a bunch in x-direction
N_{iy}	Number of floes in a bunch in y-direction
S_x	Distance between floes in x-direction
S_y	Distance between floes in y-direction
$\vec{V}_a$	Wind velocity at a height of 10 m
$\vec{v}_i$	Ice velocity
$\vec{v}_w$	Water velocity
η	Water surface elevation
η'	Water surface elevation due to ice displacement effect
μ_i	Ice/ice friction coefficient
ρ_a	Density of air
ρ_i	Density of ice
ρ_w	Density of water
$\vec{\tau}_b$	Shear stress acting on bottom of layer
$\vec{\tau}_t$	Shear stress acting on top of layer
ϕ	Latitude of interest
ω	Angular velocity of earth rotation

1. Introduction

When movement of pack ice is simulated, it is very important to evaluate the interaction among the fragments of pack ice and those among the fragments and a solid body such as a coastline or an ocean structure. So far, researchers involved with such problems have treated the pack ice as a continuum. Several continuum models have been proposed and applied to long-term and wide-area predictions[1),2),3)], and short-term and narrow-area predictions[4),5),6)]. However, since the pack ice has discrete features, such models have certain limitations. On the other hand, Serrer[7)] and Frederking & Sayed[8)] proposed a discrete element model approximating each ice floe by a circular disk. Although this approach is interesting, practical applications of it might be difficult because it requires much computation time.

A Distributed Mass / Discrete Floe (DMDF) model is a new model for numerical simulation of mesoscale pack ice rheology. It has the advantages of both a continuum model and a discrete model. It can express the discrete nature of pack ice which is difficult for a continuum model to treat. It can treat larger number of floes in much shorter computation time compared to the discrete element model.

The pack ice is divided into rectangular bunches in which the floes, all of equal size, are assumed to be distributed uniformly. The ice interaction forces are formulated from the relation between the impulse on the ice bunch and the variation of the bunch momentum. The floes are modeled as inelastic circular disks or rectangles floating on the water. The equations of bunch motion are formulated from momentum conservation law, taking into account the Coriolis force, the sea surface inclination force, the interaction forces among the floe bunches and the stress due to the wind and water current. A semi-Lagrangian ice mass transport procedure is adopted. A multi-layer model is used in simulating the flow of sea water simultaneously with the ice floe movement to account for the surface flow more accurately. Finite difference formulations of the sea water flow have been done using the MacCormack predictor-corrector scheme. Figure 1 shows the computational procedure of this model.

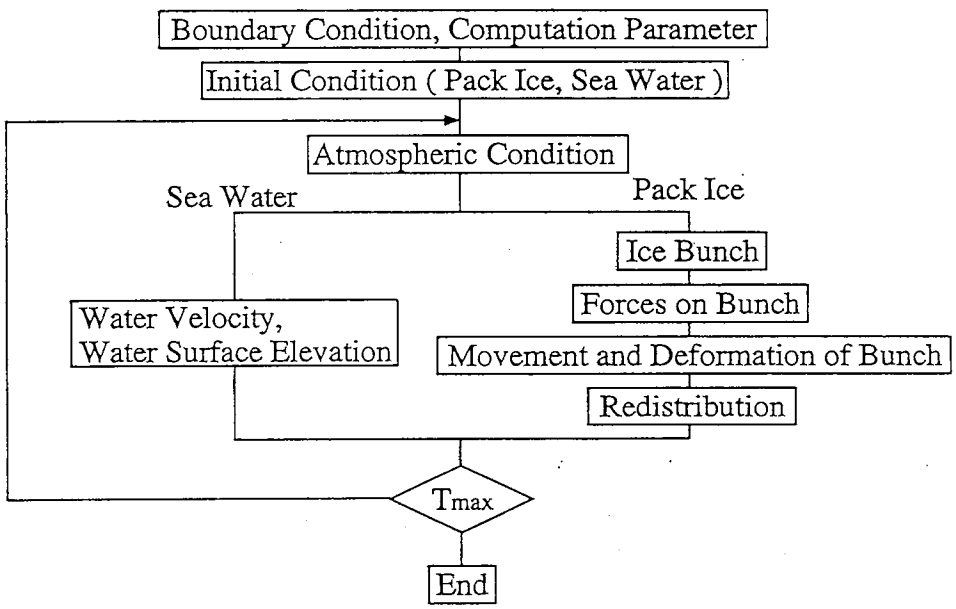

Fig. 1 Computational procedure of DMDF model

2. Ice Model

In the present model, where the orthogonal coordinate system is adopted for the ice floes movement computation, the pack ice is divided into rectangular ice bunches in which the floes, all of equal area and thickness, are assumed to be distributed uniformly. The floes are modeled as inelastic circular disks or rectangles.

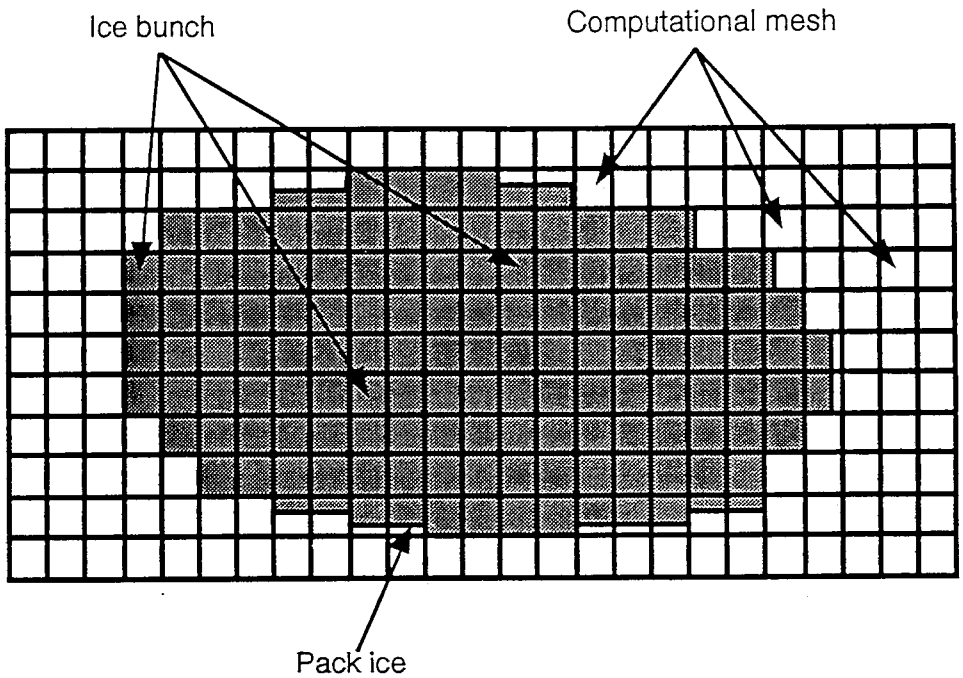

Fig. 2 Pack ice, computational mesh and ice bunch

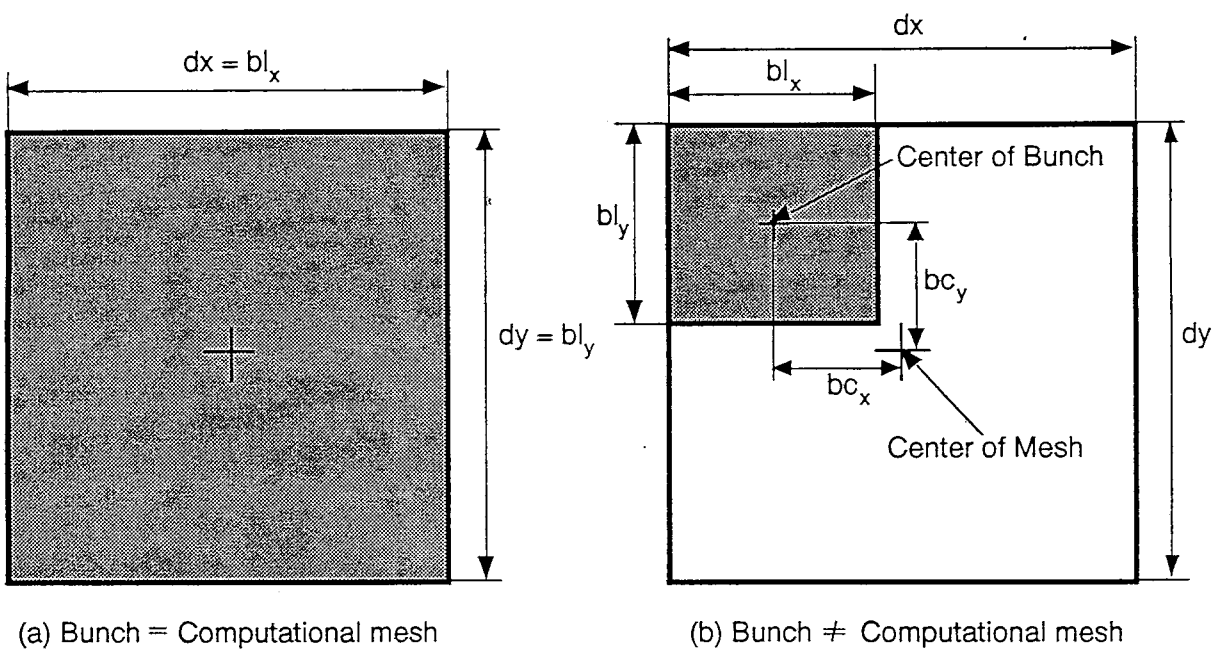

(a) Bunch = Computational mesh (b) Bunch ≠ Computational mesh

Fig. 3 Bunch and computational mesh

A bunch is characterized by the values of its center position, area and ice concentration

which is a ratio of the ice covered area to the bunch area:

$$C_i = \frac{A_i}{bl_x bl_y} \tag{1}$$

$$A_i = N_{ix} N_{iy} \frac{\pi \, dl_{ic} dl_{ic}}{4} \qquad \text{for circular disk} \tag{2-1}$$

$$A_i = N_{ix} N_{iy} dl_{ix} dl_{iy} \qquad \text{for rectangle} \tag{2-2}$$

where, C_i denotes the ice concentration of a bunch, A_i is the total surface area of floes in a bunch, $bl_x bl_y$ is the bunch area, $N_{ix} N_{iy}$ is the number of floes in a bunch, dl_{ic} is the diameter of circular disk floe and $dl_{ix} dl_{iy}$ is the surface area of a rectangle floe. Figure 4 shows two such bunches with 9 elements.

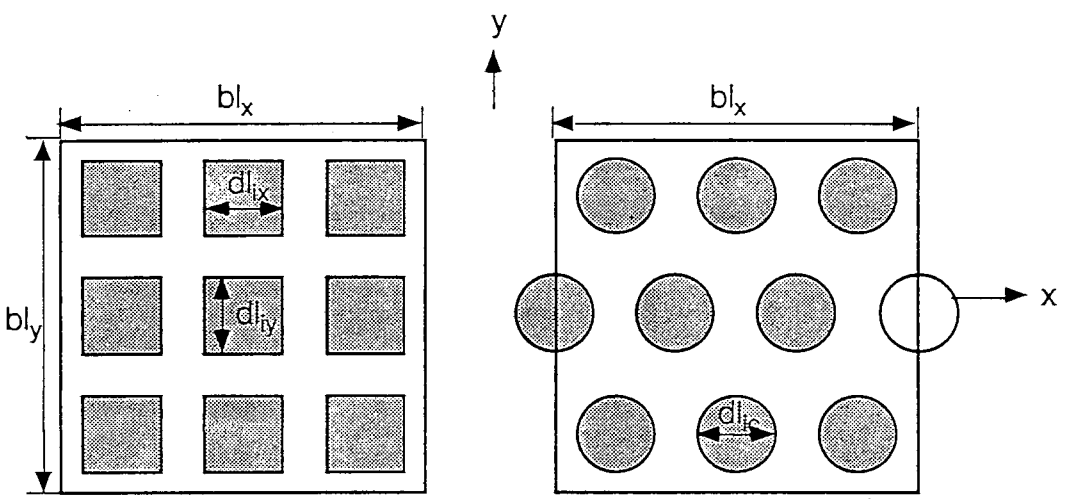

(a) Circular disk floe bunch (b) Rectangle floe bunch

Fig. 4 Floes and bunch

3. Equations of Bunch Motion

Ice floe movement with a relatively short time-scale (of the order of several days at most) can be numerically well simulated with a dynamic model where the Coriolis force, the sea-surface inclination force, the interaction forces among the floe bunches and the stress due to the wind and water current are taken into account, neglecting ice growth and ablation.

The momentum change of the ice floe bunch in a time interval of dt can be expressed by the following equation:

$$M_i(\vec{v}_i^{t+dt}-\vec{v}_i^{t})=\int_t^{t+dt}(A_i\vec{\tau}_a+A_i\vec{\tau}_w-Mg\nabla(\eta+\eta')+M_i f\vec{k}\times\vec{v}_i^{t}+\vec{F}_i)dt \tag{3}$$

where,

$$M_i=\rho_i h_i C_i bl_x bl_y \tag{4}$$

$$\vec{\tau}_a=\rho_a C_a|\vec{V}_a-\vec{v}_i|(\vec{V}_a-\vec{v}_i) \tag{5}$$

$$\vec{\tau}_w=\rho_w C_w|\vec{v}_w-\vec{v}_i|(\vec{v}_w-\vec{v}_i) \tag{6}$$

M_i is the bunch mass while $\vec{\tau}_a$ and $\vec{\tau}_w$ denote the shearing forces acting on the bunch due to the wind and the sea current respectively. $-Mg\nabla(\eta+\eta')$ is the force due to the inclination of the sea surface. $M_i f\vec{k}\times\vec{v}_i^{t}$ is the Coriolis force which acts in the right-hand direction perpendicular to the bunch movement in the Northern Hemisphere. $\vec{F}_i$ denotes the ice internal force, i.e. the interaction force of floes in a bunch and between bunches. This is the force due to the mutual collision and separation between the floes.

4. Ice Interaction Force

4.1 Axial ice interaction

The axial interaction forces are formulated from the relation between the impulse on the bunch and the variation of the bunch momentum, the ice floes being treated as rigid bodies. Two ice bunches are considered in figure 5. The velocity of bunch A relative to bunch B is expressed by,

$$v_s=v_i^A-v_i^B \tag{6}$$

In case that $v_s dt-dl-(S_x^A+S_x^B)/2$ is positive (dl is the spacing between bunches. S_x^A and S_x^B denote the distance between floes in x-direction of the bunch A and the bunch B, respectively), the bunch A collides with the bunch B within one time step of dt. The number of ice floes in a bunch A, which take part in the collision with the neighboring bunch, is an integer n_x^A satisfying the inequality,

$$(n_x^A-1)S_x^A\le v_s dt-dl-(S_x^A+S_x^B)/2<n_x^A S_x^A \tag{7}$$

$n_x^A=0$, if n_x^A becomes less than 1. Letting $n_x^A N_{iy}^A$ be the number of them to collide with the neighboring bunch B, the axial momentum change of the bunch A due to the collision is expressed by,

$$\int_t^{t+dt}\vec{F}_{ix}dt=m_i^A(v_i'-v_i^A) \tag{8}$$

$$v_i'=\frac{m_i^A v_i^A+m_i^B v_i^B}{m_i^A+m_i^B} \tag{9}$$

$$m_i^A=\frac{n_x^A}{N_{ix}^A}M_i^A \tag{10}$$

where, m_i^A is the mass of the floes taking part in the collision.

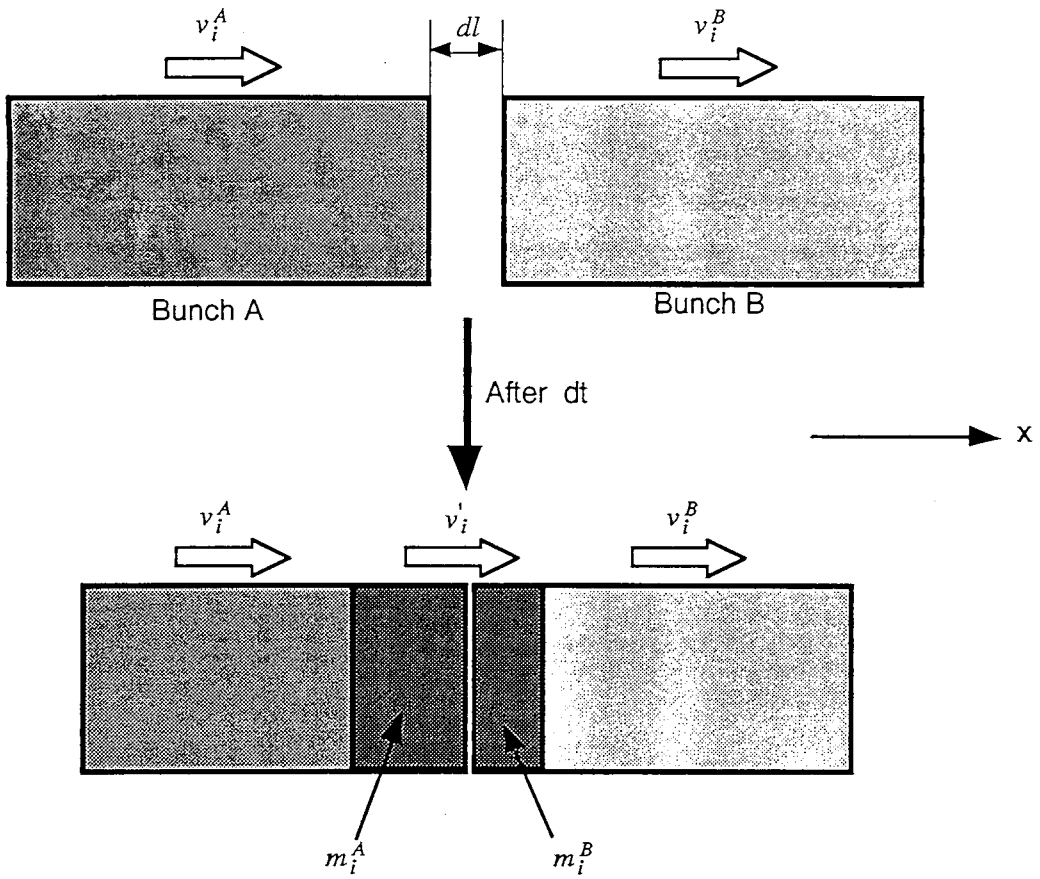

Fig. 5 Axial collision between bunches

4.2 Lateral expansion of floes

An ice bunch moving against a fixed boundary is considered in Figure 6 in which four rows of floes in the bunch collide with the fixed boundary. From the force equilibrium, the interaction forces between floes are expressed by following equations,

$$F_i^{12}=\frac{F_b(\sin\theta-\mu_i\cos\theta)}{2(\cos\theta+\mu_i\sin\theta)} \tag{11-1}$$

$$F_i^{23}=F_i^{12}+\frac{F_b(\sin\theta-\mu_i\cos\theta)}{2(\cos\theta+\mu_i\sin\theta)} \tag{11-2}$$

$$F_i^{34}=F_i^{23}+\frac{F_b(\sin\theta-\mu_i\cos\theta)}{2(\cos\theta+\mu_i\sin\theta)} \tag{11-3}$$

$$F_i^{4B}=F_i^{34}+\frac{F_b(\sin\theta-\mu_i\cos\theta)}{2(\cos\theta+\mu_i\sin\theta)} \tag{11-4}$$

where F_b is the body force on a floe, μ_i is the friction coefficient between floes and θ is the angle between the direction of progress of a floe and the collision direction with another floe. The angle of θ is a function of the ice concentration and floe shape. It is larger than 30° for the

case of a circular disk floe and it becomes zero for the case of a rectangle floe. In the DMDF model, the shape of the floes is taken into consideration as the value of the angle of θ.

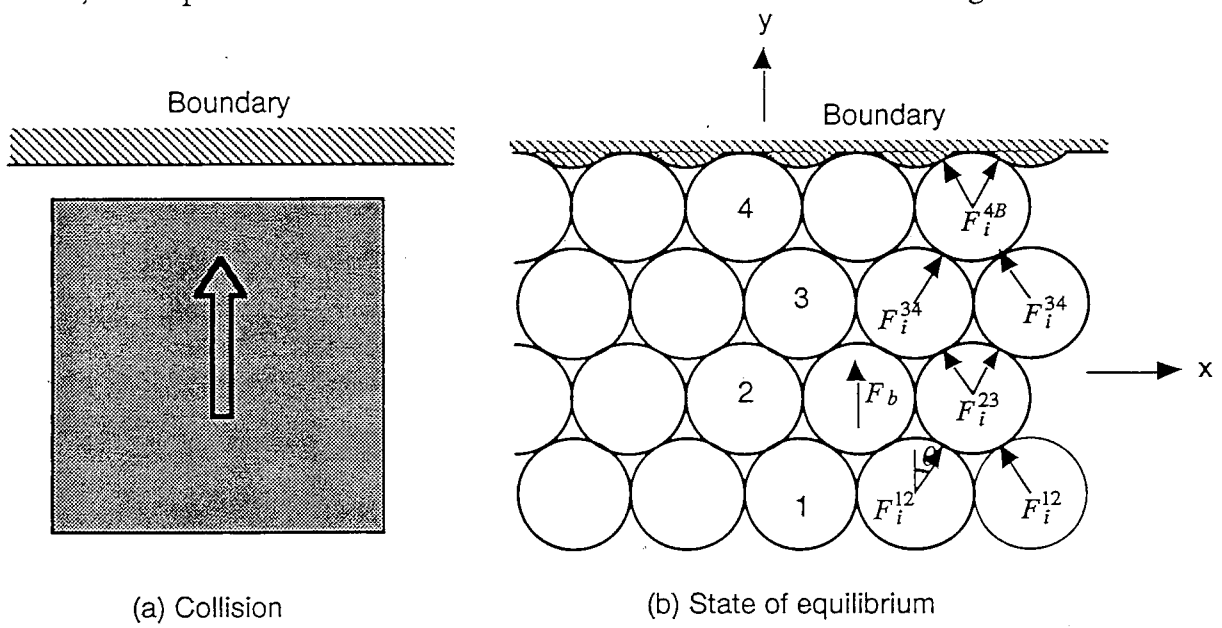

Fig. 6 Lateral expansion of floes

Due to the interaction forces, the floes break away from the group sequentially. First, the ice floes 1 and 3 (Figure 7 (a)) depart with an impulse $F_{ix}^{o}dt_1^{o}$ given by,

$$F_{ix}^{o}dt_1^{o}=(F_i^{12}+F_i^{23}+F_i^{34})(\sin\theta-\mu_i\cos\theta)\cdot dt_1^{o}$$
$$=\frac{(1+2+3)F_b(\sin\theta-\mu_i\cos\theta)}{2(\cos\theta+\mu_i\sin\theta)}dt_1^{o} \qquad (12)$$

where dt_1^{o} is the time taken by the floe 1 and 3 to depart from the group. Second, the floes 2 and 4 (Figure 7 (a)) do the same with a combined impulse $F_{ix}^{e}dt_1^{e}$ given by,

$$F_{ix}^{e}dt_1^{e}=(F_i^{12}+F_i^{23}+F_i^{34}+F_i^{4B})(\sin\theta-\mu_i\cos\theta)\cdot dt_1^{e}$$
$$=\frac{(1+2+3+4)F_b(\sin\theta-\mu_i\cos\theta)}{2(\cos\theta+\mu_i\sin\theta)}dt_1^{e} \qquad (13)$$

where dt_1^{e} is the time taken by the floes 2 and 4 to depart after the floe 1 and 3 departed. Third, the ice floes 1' and 3' depart with the impulse $F_{ix}^{o}dt_2^{o}$ followed by 2' and 4', thus repeating the sequence. A half of ice floes to collide with the boundary, move to the right side of the bunch and the others move to the left side. This lateral movement is called "Lateral Expansion of Floe". Expressing the number of floe rows to collide with the fixed boundary in y-direction as n_{iy}, the number of floes which move to right side is $n_{iy}N_{ix}/2$ and the total expansion momentum directed to the right side of the bunch is expressed as follows,

$$F_{ixe}^{R}dt=F_{ix}^{o}dt_1^{o}+F_{ix}^{e}dt_1^{e}+F_{ix}^{o}dt_2^{o}+F_{ix}^{e}dt_2^{e}+\cdots\cdots+F_{ix}^{o}dt_{N_{ix}/2}^{o}+F_{ix}^{e}dt_{N_{ix}/2}^{e} \qquad (14)$$

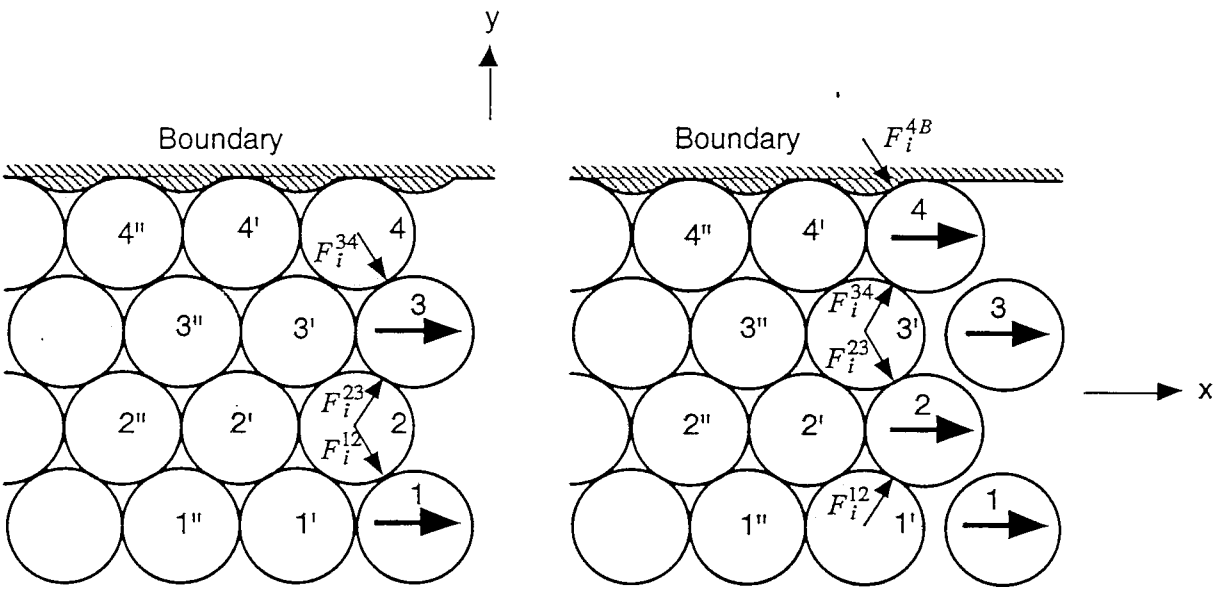

(a) The First step (b) The Second step

Fig. 7 Procedure of floe expansion

where

$$dt=dt_1^o+dt_1^e+dt_2^o+dt_2^e+\cdots\cdots+dt_{N_{ix}/2}^o+dt_{N_{ix}/2}^e \tag{15}$$

$$F_{ix}^o=\frac{\{1+2+\cdots+(n_{iy}-1)\}F_b(\sin\theta-\mu_i\cos\theta)}{2(\cos\theta+\mu_i\sin\theta)} \tag{16}$$

$$F_{ix}^e=\frac{\{1+2+\cdots+n_{iy}\}F_b(\sin\theta-\mu_i\cos\theta)}{2(\cos\theta+\mu_i\sin\theta)} \tag{17}$$

Assuming that

$$dt_1^o=dt_1^e=dt_2^o=dt_2^e=\cdots\cdots=dt_{N_{ix}/2}^o=dt_{N_{ix}/2}^e=\frac{dt}{N_{ix}} \tag{18}$$

the expansion momentum directed to the right side becomes

$$F_{ixe}^R dt=(F_{ix}^o+F_{ix}^e)\frac{dt}{2}=\frac{n_{iy}\cdot n_{iy}\cdot F_b(\sin\theta-\mu_i\cos\theta)}{4(\cos\theta+\mu_i\sin\theta)}dt \tag{19}$$

The equation (18) is justified because the phenomenon is periodical in x-direction. Since the total mass of the floes which expand to the right side is $M_i \cdot n_{iy}/N_{iy}/2$, the acceleration of them becomes $F_{ixe}^R/(M_i \cdot n_{iy}/N_{iy}/2)=2F_{ixe}^R \cdot N_{iy}/(M_i \cdot n_{iy})$. Thus, the right edge moves to the right side with a distance $F_{ixe}^R \cdot N_{iy} \cdot dt^2/(M_i \cdot n_{iy})$ in the time interval of dt. The left edge moves to the left side with the same distance. As a result, after the time step of dt the x-direction length of the bunch becomes

$$bl_x^{t+dt} = bl_x^t + 2\frac{F_{ixe}^R \cdot N_{iy}}{M_i \cdot n_{iy}} dt^2 \tag{19}$$

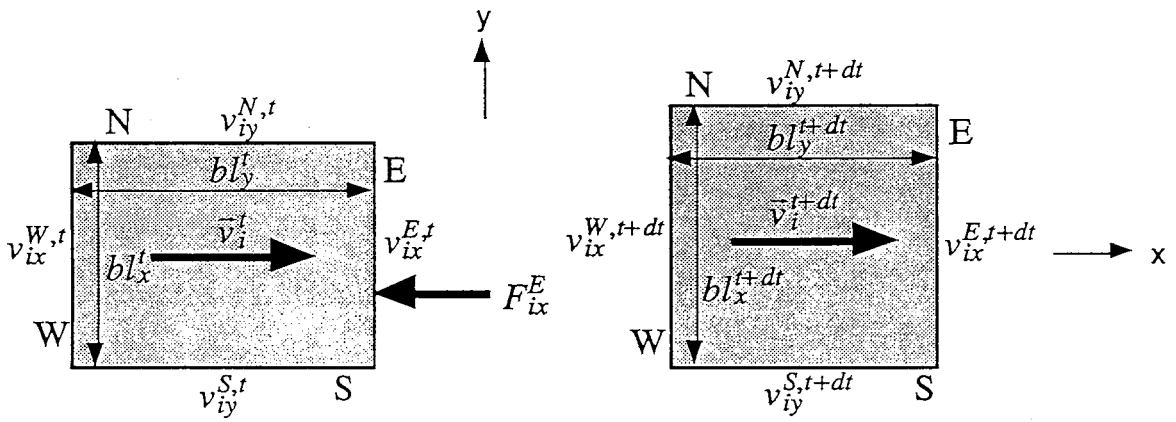

Fig. 8 Movement and deformation of bunch

5. Movement and Deformation of Bunch

The bunches move following the above equations and change shapes due to the interaction. In the present model, the bunch movement and deformation are expressed by the movement of the four edges of bunch. One bunch whose size and velocity at the time t are $bl_{ix}^t bl_{iy}^t$ and $\bar{v}_i^t$ respectively, is considered in Figure 8. The bunch collides with the neighboring bunch within one time step of dt. The axial interaction force exerted on the edge of E is F_{ix}^E.

The y-direction lateral expansion force exerted on the edge of N and S are expressed by,

$$F_{iy}^N = -F_{iy}^S = \frac{n_{ix} \cdot F_{ix}^E (\sin\theta - \mu_i \cos\theta)}{4N_{iy}(\cos\theta + \mu_i \sin\theta)} \tag{20}$$

Assuming that the force exerted on the floes except the interaction force is $\bar{F}_b$, the velocity of the edges of the bunch at time $t+dt$ are expressed as,

$$v_{ix}^{E,t+dt} = v_{ix}^{E,t} - \left(\frac{F_{ix}^E}{n_{ix}} - F_{bx} \cdot N_{iy}\right)\frac{dt \cdot N_{ix}}{M_i} \tag{21}$$

$$v_{ix}^{W,t+dt} = v_{ix}^{W,t} + F_{bx} \cdot N_{iy}\frac{dt \cdot N_{ix}}{M_i} \tag{22}$$

$$v_{iy}^{N,t+dt} = v_{iy}^{N,t} + \left(\frac{2F_{iy}^N}{N_{iy}} + F_{by} \cdot N_{ix}\right)\frac{dt \cdot N_{iy}}{M_i} \tag{23}$$

$$v_{iy}^{S,t+dt}=v_{iy}^{S,t}+(\frac{2F_{iy}^{S}}{N_{iy}}+F_{by}\cdot N_{ix})\frac{dt\cdot N_{iy}}{M_i} \tag{24}$$

Assuming that the velocity of the edges varies linearly, the moving distances of the edges are determined by the following equations,

$$\Delta x_i^E=v_{ix}^{E,t}dt-(\frac{F_{ix}^E}{n_{ix}}-F_{bx}\cdot N_{iy})\frac{N_{ix}}{M_i}\frac{dt\cdot dt}{2} \tag{25}$$

$$\Delta x_i^W=v_{ix}^{W,t}dt+F_{bx}\cdot N_{iy}\frac{N_{ix}}{M_i}\frac{dt\cdot dt}{2} \tag{26}$$

$$\Delta y_i^N=v_{iy}^{N,t}dt+(\frac{n_{ix}\cdot F_{ix}^E(\sin\theta-\mu_i\cos\theta)}{2N_{iy}\cdot N_{iy}(\cos\theta+\mu_i\sin\theta)}+F_{by}\cdot N_{ix})\frac{N_{iy}}{M_i}\frac{dt\cdot dt}{2} \tag{27}$$

$$\Delta y_i^S=v_{iy}^{S,t}dt-(\frac{n_{ix}\cdot F_{ix}^E(\sin\theta-\mu_i\cos\theta)}{2N_{iy}\cdot N_{iy}(\cos\theta+\mu_i\sin\theta)}-F_{by}\cdot N_{ix})\frac{N_{iy}}{M_i}\frac{dt\cdot dt}{2} \tag{28}$$

and the size of the bunch changes as follows:

$$bl_x^{t+dt}=bl_x^t-\frac{F_{ix}^E}{n_{ix}}\frac{N_{ix}}{M_i}\frac{dt\cdot dt}{2} \tag{29}$$

$$bl_y^{t+dt}=bl_y^t+\frac{n_{ix}\cdot F_{ix}^E(\sin\theta-\mu_i\cos\theta)}{M_i\cdot N_{iy}(\cos\theta+\mu_i\sin\theta)}\frac{dt\cdot dt}{2} \tag{30}$$

6. Redistribution of Pack Ice

The bunches move following the above equations. As a result, the edge of the respective bunches do not coincide with the edges of the computation mesh after the movement in the interval of dt. Therefore, the floes are redistributed into one bunch for one mesh, conserving the mass and momentum. The characteristics values of the new bunch are determined by the following equation;

$$bl_x^{j,t+dt}=x_{\max}^j-x_{\min}^j \tag{30-1}$$

$$bl_y^{j,t+dt}=y_{\max}^j-y_{\min}^j \tag{30-2}$$

$$bc_x^{j,t+dt}=\frac{x_{\max}^j+x_{\min}^j}{2} \tag{30-3}$$

$$bc_y^{j,t+dt}=\frac{y_{\max}^j+y_{\min}^j}{2} \tag{30-4}$$

$$C_i^j=\sum_{k=1}^{n_b}C_i^{j,k} \tag{30-5}$$

$$C_i^j h_i^j bl_x^{j,t+dt}bl_y^{j,t+dt}=\sum_{k=1}^{n_b}C_i^{j,k}h_i^{j,k}bl_x^{j,k,t+dt}bl_y^{j,k,t+dt} \tag{30-6}$$

$$C_i^j h_i^j bl_x^{j,t+dt}bl_y^{j,t+dt}\bar{v}_i^{j,t+dt}=\sum_{k=1}^{n_b}C_i^{j,k}h_i^{j,k}bl_x^{j,k,t+dt}bl_y^{j,k,t+dt}\bar{v}_i^{j,t+dt} \tag{30-7}$$

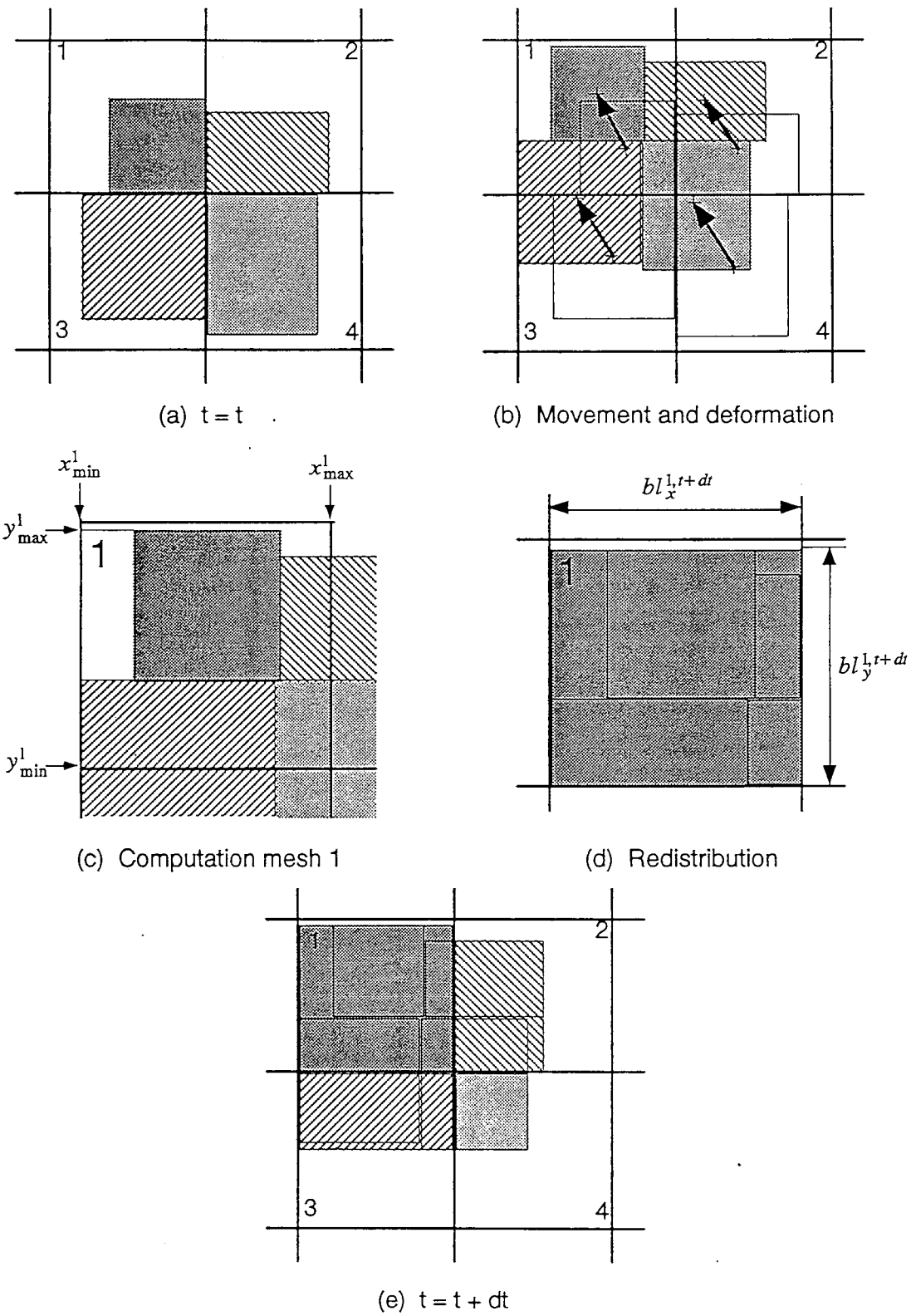

Fig. 9 Redistribution of pack ice

where, n_b is the number of bunches which came into the computation mesh under consideration as shown in Figure 9. Equations (30-5), (30-6) and (30-7) express the ice concentration, mass and momentum conservation, respectively.

7. Ocean Flow

For the ice movement, it is important to analyze the ocean flow, particularly near the sea surface. In the present computation, the ocean flow is divided into horizontal layers as shown in Figure 10. The momentum conservation equations (the Navier-Stokes equations integrated in the layer height) and the continuity equation are

$$\frac{\partial q_{wx}}{\partial t}+v_{wx}\frac{\partial q_{wx}}{\partial x}+v_{wy}\frac{\partial q_{wx}}{\partial y}-f q_{wy}$$
$$=-g\frac{\partial(\eta+\eta')d_{zk}}{\partial x}+\frac{\tau_{tx}+\tau_{bx}}{\rho_w}+2E_{xx}\frac{\partial^2 q_{wx}}{\partial x^2}+E_{yx}\frac{\partial}{\partial y}\left(\frac{\partial q_{wx}}{\partial x}+\frac{\partial q_{wy}}{\partial y}\right) \quad (31)$$

$$\frac{\partial q_{wy}}{\partial t}+v_{wx}\frac{\partial q_{wy}}{\partial x}+v_{wy}\frac{\partial q_{wy}}{\partial y}+f q_{wx}$$
$$=-g\frac{\partial(\eta+\eta')d_{zk}}{\partial y}+\frac{\tau_{ty}+\tau_{by}}{\rho_w}+2E_{yy}\frac{\partial^2 q_{wy}}{\partial y^2}+E_{xy}\frac{\partial}{\partial x}\left(\frac{\partial q_{wx}}{\partial x}+\frac{\partial q_{wy}}{\partial y}\right) \quad (32)$$

$$\frac{\partial \eta}{\partial t}+\frac{\partial Q_{wx}}{\partial x}+\frac{\partial Q_{wy}}{\partial y}=0 \quad (33)$$

where d_{zk} is the height of the k-th layer, and

$$q_{wx}=v_{wx}d_{zk},\quad q_{wy}=v_{wy}d_{zk}$$
$$Q_{wx}=\int_{-h}^{\eta}v_{wx}dz,\quad Q_{wy}=\int_{-h}^{\eta}v_{wy}dz$$

q_{wx} and q_{wy} are water fluxes in x- and y-direction in the layer, and Q_{wx} and Q_{wy} are total water fluxes.

For $k=1$, the shearing stress on the top becomes,

$$\vec{\tau}_t=C_i\vec{\tau}_w+(1-C_i)\vec{\tau}_{aw} \quad (34)$$

where,

$$\vec{\tau}_{aw}=\rho_a C_d|\vec{V}_a|\vec{V}_a \quad (35)$$

is the shearing stress between the water and air, and $\vec{\tau}_w$ is the stress between the water and ice given by the equation (6).

The equation of Wu[9] is used for the friction coefficient C_d due to wind on the water surface,

$$C_d=(0.8+0.065|\vec{V}_a|)\times10^{-3} \quad (36)$$

For $k=2$ to $k_{\max}$,

$$\vec{\tau}_t^{k-1} = -\vec{\tau}_b^{k} = \rho_w E_z \frac{\partial \vec{v}_w}{\partial z} \tag{37}$$

with the no slip condition on the seabed. The eddy viscosity E_z is obtained by multiplying the grid spacing and ice concentration parameter with E_{zo},

$$\rho_w E_{zo} = \begin{Bmatrix} 0.114|\vec{V}_a|^3 & |\vec{V}_a| < 4m/\sec \\ 5.584|\vec{V}_a| - 15.04 & 4m/\sec \le |\vec{V}_a| \le 8m/\sec \\ 0.463|\vec{V}_a|^2 & 4m/\sec < |\vec{V}_a| \end{Bmatrix} \tag{38}$$

The above equation is a modified form of the observation equations of Ekman and Thorade[10]. Finite difference formulations of the ocean flow were made using the MacCormack predictor-corrector scheme[11].

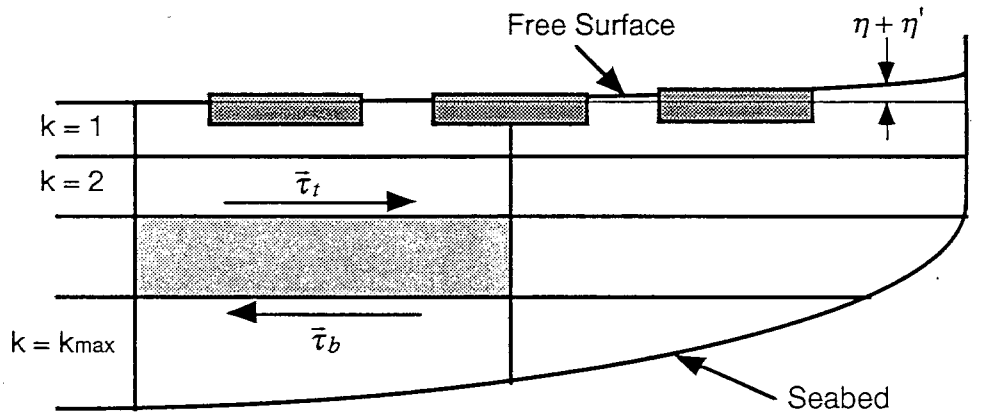

Fig. 10 Modeling of ocean flow

Summary and Conclusions

The Distributed Mass / Discrete Floe model is a numerical model proposed for the computation of mesoscale pack ice rheology with the difference of floe shape taken into consideration. This model possesses the advantages of both the continuum and the discrete element ones: it can express the discrete nature of pack ice which is difficult for a continuum model to treat, and can realize much shorter computation time than a discrete element model.

The pack ice is divided into rectangular bunches in which the floes, all of equal size, are assumed to be distributed uniformly. The ice interaction forces are formulated from the relation between the impulse on the ice bunch and the variation of the bunch momentum. The floes are modeled as inelastic circular disks or rectangles floating on the water. The equations of bunch motion are formulated from momentum conservation law, taking into account the

Coriolis force, the sea surface inclination force, the interaction forces among the floe bunches and the stress due to the wind and water current. A semi-Lagrangian ice mass transport procedure is adopted. A multi-layer model is used in simulating the flow of sea water simultaneously with the ice floe movement to account for the surface flow more accurately. Finite difference formulations of the sea water flow have been done using the MacCormack predictor-corrector scheme.

References

1) Campbell, W.J., "The Wind-Driven Circulation of Ice and Water in a Polar Ocean", J Geophys Res, Vol. 70, No. 4, pp. 3279-3301, 1965.
2) Hibler III, W.D., "A Dynamic Thermodynamic Sea Ice Model", J Phys Oceanogr, Vol. 9, pp. 815-846, 1979.
3) Flato, G.M. and W.D. Hibler III, "Modeling Pack Ice as a Cavitating Fluid", J Phys Oceanography, Vol. 22, pp. 626 - 651, 1992.
4) Thomson, N.R., J.K. Sykes and R.F. McKenna, "Short-Term Ice Motion Modeling with Application to the Beaufort Sea", J Geophys Res, Vol. 93, pp. 6819 - 6836, 1988.
5) Bruno, M.S. and O.S. Madsen, "Coupled Circulation and Ice Floe Movement Model for Partially Ice-Covered Continental Shelves", J Geophys Res, Vol. 94, pp. 2065 - 2077, 1989.
6) Rheem, C.K., H. Yamaguchi, H. Kato and H. Horikome, "A Numerical Study on Pack Ice Movement Using a Dynamic Ice Model as a Continuum", J Soc Naval Archi Jpn, Vol. 173, pp. 169 - 174, 1993.
7) Serrer, M., S.B. Savage and M. Sayed, "Visualization of Marginal Ice Zone Dynamics", Proc 1st Int Conf and Exhibution VIDEA 93, Southampton, UK, 1993.
8) Frederking, R. and M. Sayed, "Numercal Simulations of Mesoscale Rheology of Broken Ice Fields", Proc 12th Int Conf POAC, Vol. 2, pp. 789 - 798, 1993.
9) Wu, J., "Wind-Stress Coefficients over Sea surface from Breeze to Hurricane", J Geophys Res, Vol. 87, pp. 9704 - 9706, 1982.
10) Thorade, H., "Die Geschwindigkeit von Triftomungen und die Ekmansche Theorie", Ann d Hydrogr u Mar Meteor, Bd. 42, pp. 379 - 391, 1914.
11) Hoffmann, K.A., "Computational Fluid Dynamics for Engineering", Engineering Education System, Austin, pp. 220-221, 1989.

PART II : Model Verification
- Comparison to Circulation Water Channel Experiments and Sea Ice Motion in the Southern Part of the Okhotsk -

Abstract

In a circulation water channel, drift tests of physical model floes were performed in order to investigate the characteristics of their motion and interaction with the structure. The floe motion near the structure depends on the floe shape. Disk floes show a lateral motion in front of the structure. They flow out from both sides of the structure and the number of floes in front of the structure decreases with time. On the other hand, rectangle floes scarcely expand laterally. The number of the floes in front of the structure remains almost constant with respect to time. These experiments indicate that when the motion of pack ice is simulated around a structure, it is important to choose the floe shape. The disk floe motion and the rectangle floe motion can be regarded as the two extreme cases of pack ice motions. An actual pack ice motion may be between these two extreme cases.

Some computations using Distributed Mass / Discrete Floe (DMDF) model were made. Simulation results were compared with the circulating water channel experiments and the sea ice motion in the southern part of the Okhotsk. The DMDF predicted the circulating water channel drift tests quite closely. The DMDF results also compared quite well with the sea ice motion.

1. Introduction

The pack ice motion near the ocean structure depends on the floe shapes and the structure. The collision between disks is along the diametral line. On the other hand, rectangles collide facially. As a result, the motion of disks floes is more active than rectangles near the structure. When the structure stops both the floes and water, the floes decrease their speed in front of the structure because the water stagnates in front of the structure.

Even though several models have been proposed for forecasting pack ice motion, calibration data are scanty. This study investigates experimentally the characteristics of the pack ice motion and the interaction among the fragments of pack ice and those among the fragments and a solid body such as an ocean structure for different floe shapes. The drift tests using disk and rectangle physical model floes are performed in a circulation water channel. The floes were driven by the wind and the current.

Two computations are made in order to investigate characteristics of pack ice motion with Distributed Mass / Discrete Floe model. One is made for the same conditions as the drift tests of the physical model floes around an ocean structure made at the circulating water channel. The other is sea ice motion simulation in the southern part of the Okhotsk. Simulation results are compared with the sea ice motion.

2. Drift Tests of Physical Model Floes

The aim of the drift test of model floes was to investigate the characteristics of floe motion and interaction between floe and ocean structure for different floe shapes.

2.1 Experimental set-up

The experiments were performed in a circulation water channel equipped with wind blower at the Chiba Experiment Station, Institute of Industrial Science, University of Tokyo. The test section is 8 m long × 1.8 m wide × 0.9 m deep. Figure 1 shows the principal arrangement for these tests.

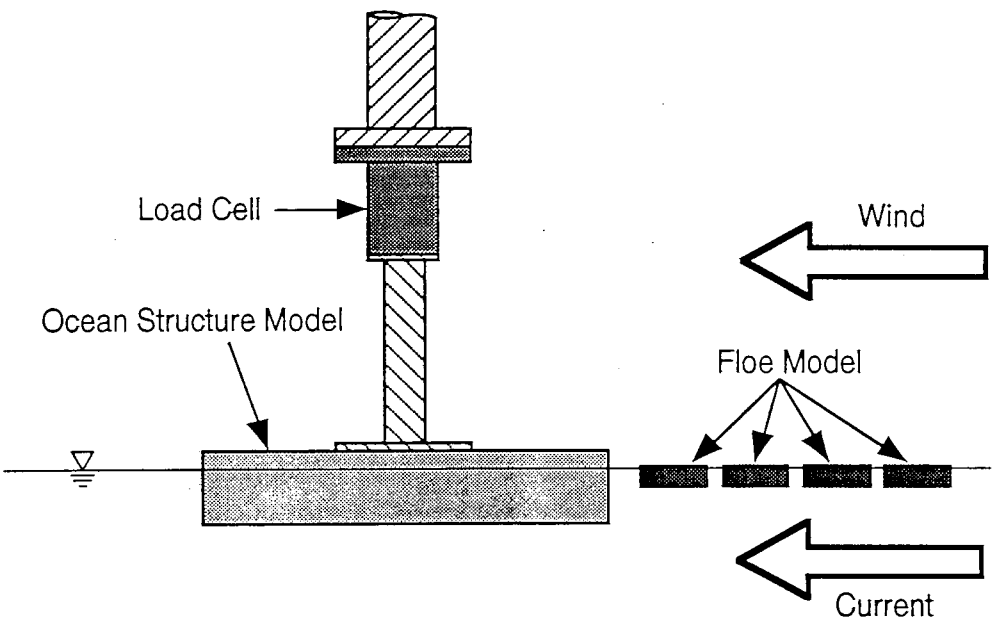

Fig. 1 Measurement system arrangement for an ocean structure model

The disk and rectangle physical model floes were made of polypropylene with a specific weight of 0.912. The size of the disk was 50 mm diameter × 15 mm deep and that of the rectangle was 50 mm × 50 mm × 15 mm deep. Two ocean structure models of size 300

mm × 300 mm × 50 mm deep were used. One was made from a stainless steel mesh to pass water. The other was made from a board to stop water.

A three-component dynamometer was used to measure the ice interaction force of Fx, Fy and Mz on the structure. Figure 2 shows the measuring section and the initial conditions of the tests.

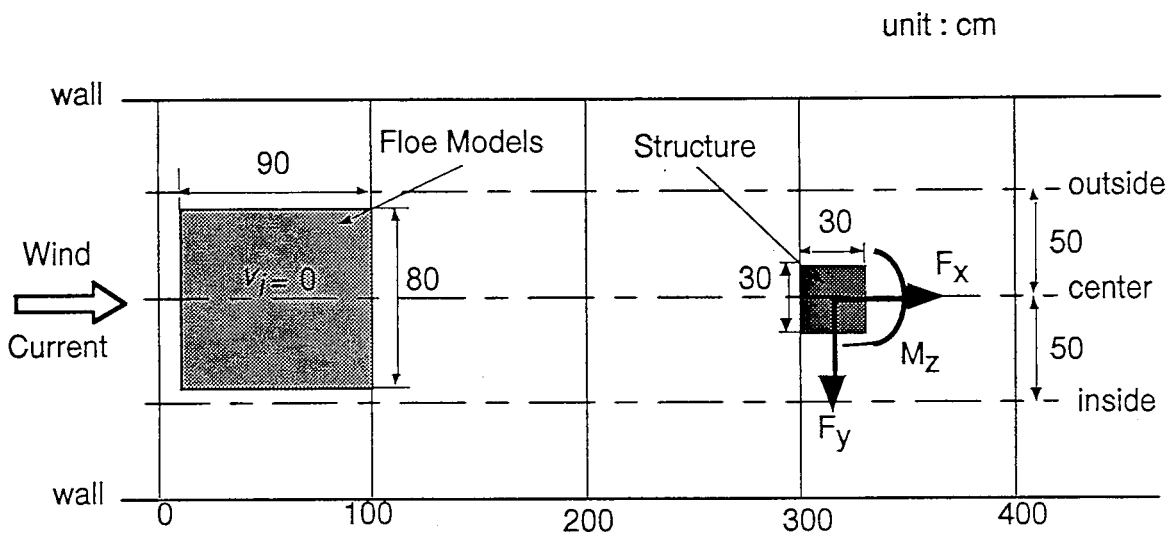

Fig. 2 Measuring section and initial condition of drift test of floe models around an ocean structure model of size 300 mm × 300 mm × 50 mm deep

2.2 Wind and current distribution

All the experiments were made under the same wind and current conditions. Figures 3 and 4 show the measured wind and current distribution in the absence of floe on the water surface. The wind speed was measured by a Pitot tube anemometer at a height of 50 mm above the water surface, and the water speed was measured by a blade wheel current meter at a depth of 15 mm.

The wind blows slightly stronger at the inside and outside of the channel than at the center. The reason is that the blower has two fans whose centers are near the inside and outside positions of the channel. The current is also slightly stronger at the inside and outside of the channel than at the center because of the difference in wind; and the water speed is higher downstream than upstream since the water has been accelerated by the wind.

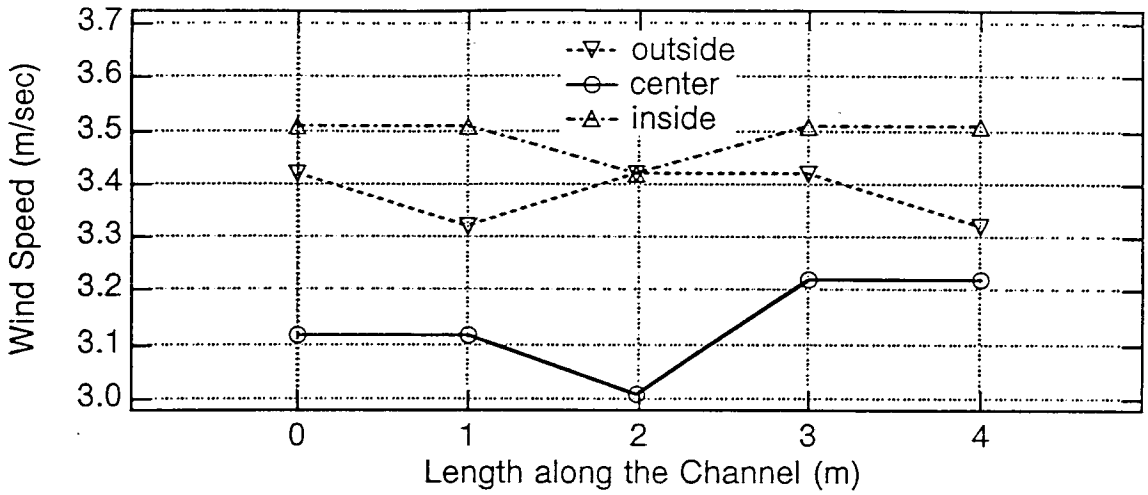

Fig. 3 Wind distribution

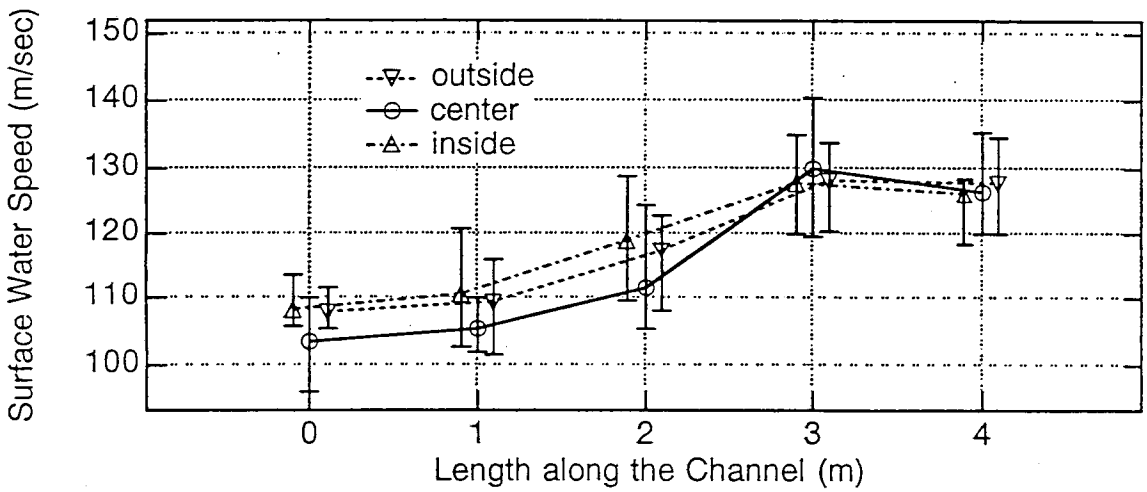

Fig. 4 Current distribution

3. Experimental Results

3.1 Free drift of physical model floes

Initially, the model floes were located at the upstream center of the channel with the area of 800 mm × 900 mm as shown in Figure 2. The initial concentration of model floes was 0.99 for the case of rectangles and 0.9 for disks. The floes were at rest and the wind and current were steady. The surface water reduced speed at the center of the channel, because the floes were at rest. The initial surface water speed at the position of the structure was reduced to 93.5 m/sec for the case of disks and 98.5 mm/sec for rectangles due to the drag of the model

floes. The floes begin to drift driven by the wind and current.

Figures 5, 6 and 7 show the time variation of drift of the model floes in the absence of the structure, for the case of disks, rectangles and mixture of disks and rectangles, respectively. The drift speed at the inside and outside of the channel is higher than at the center due to the difference of the surface water speed. In the case of the disks, the floes expand to the wall direction due to the lateral expansion force. In the case of rectangles, however, the floes scarcely expand to the wall direction and turn clockwise and counterclockwise forming two groups due to the effect of the surface tension of the water between the rectangles. In the case of mixture of disks and rectangles, the floes show intermediate behavior between the above two cases.

3.2 Drift of physical model floes around no water stop structure

The initial conditions of these tests are the same as those of the previous tests. The ocean structure model was made from a stainless steel mesh to pass water. The floes begin to drift driven by the wind and current, and some of them collide with the structure. Then the floes accumulate in front of the structure.

Figures 8 and 9 show the time variation of drift of the disk floes and the rectangle floes, respectively. In the case of the disk floes, the floes in front of the structure are in active motion, because collision between disks is along the diametral line. As a result, they flow out from both sides of the structure and the number of floes in front of the structure decreases with time. In the case of the rectangle floes, however, the floes have no motion in front of the structure, because they collide facially. The number of floes in front of the structure is almost constant with respect to time.

Figure 10 shows the time variation of the x-direction interaction force of Fx, exerted on the structure (see Figure 2). Each peak corresponds to a collision of a floe model or floe models. The horizontal axis denotes the elapsed time from the start of the drift. The negative peaks are due to the vibration of the structure. In the present tests, all the floes in front of the structure collided with the structure simultaneously, because the floe concentration was very high. Hence higher peaks appear intensively at the beginning of contact. In the case of the rectangle floes, the force Fx is stable compared to the case of the disk floes. This is due to the behavior of their motion in front of the structure: the rectangle floes had no motion, while the disk floes were in active motion. The elapsed time from the start of the drift to the first contact of the floes with the structure is about 21 seconds for disks and 18 seconds for rectangles.

3.3 Drift of physical model floes around water stop structure

In this test, the water stop ocean structure model was used with the water stop column which has the same horizontal section area as that of the structure. Figure 11 shows the configuration. The initial conditions of this test are the same as those of the previous tests except for the current distribution. The surface current distribution changed due to the water stop structure and column as shown in Figure 11 (b).

Figure 12 shows the time variation of drift of the disk floes, and Figure 13 shows the time variation of the x-direction interaction force of Fx, exerted on the structure. The floes decrease their speed and begin to move to the wall direction in front of the structure because the water stagnates in front of the structure. Then, the first contact of the floes with the structure being delayed, the highest peak value of the interaction force on the structure decreases and the number of floes which flow out from both sides increases, compared with the case when the structure stops only the floes. The elapsed time from the start of the drift to the first contact of the floes with the structure is about 24 seconds and the region of the accumulated floes in front of the structure is scarcely formed.

4. Motion Simulations of the Physical Model Floes

The movements of the physical model floes were numerically simulated using Distributed Mass / Discrete Floe model with the same conditions as the drift test of the physical model floes made in the circulating water channel.

4.1 Computation parameters

The computation mesh size was 150 mm × 150 mm. The number of water layers was 5 and the height of each layer was 30 mm. The measured speed of the current at 150 mm depth was used as the bottom condition. The friction coefficient C_w was 0.2 for both the disk and rectangle floe models and C_a was 0.013 for the disk and 0.016 for the rectangle. These values were obtained from drag measurements on a single model floe. C_a was determined in such a way that the computed single floe motion agreed with the experimental one. In the present computation, assuming that the friction coefficients were the functions of ice concentration, the following equations were used;

$$C'_{k*} = C_k((1 - fac_k \cdot C_i^+) + (1 - fac_k \cdot C_i)(N_{i*} - 1)) / N_{i*} \quad (1)$$

where subscript k denotes a kind of friction and * denotes a direction, and superscript + denotes a upstream neighboring mesh. The parameter of fac_k depends on the kind of friction and the shape of floe. The values of fac_k used in the present computation are shown in Table

1. These equations were formulated in such a way that the computed surface water speed at the position of the structure agree with the experiment. The other conditions such as the size of the computation domain, model floes and ocean structures, and the wind distribution were the same as those of the experiment.

Table 1 Friction parameters, fac_k

	C_w	C_a	C_d
Disk	0.46	0.86	1.0
Rectangle	0.78	0.80	1.0

4.2 Drift of physical model floes around no water stop structure

Initially, the floes were located at the upstream center of the channel with the area of 800 mm × 900 mm as shown in Figure 2. The ocean structure stopped only floes and the initial concentration of model floes was 0.99 for the case of rectangles and 0.9 for disks. The floes were at rest and the wind and current were steady.

Figure 14 shows the time variation of floe distribution. The results are similar to the circulating water channel experiment. In the case of the disk floes shown in Figure 14 (a), the floes accumulate in front of the structure and flow out from both sides. The number of floes in front of the structure decreases with time. The number of rectangle floes in front of the structure remains constant with time as observed. The drift speed at the inside and outside of the channel is higher than the center for both cases of disk and rectangle floes.

In the experiment, the disks expanded to the wall direction, and the rectangles turned clockwise and counterclockwise forming two groups. In the computation, however, the rotation of the floes, the surface tension of water between floes and the waves on the water surface were disregarded. And the ocean structure regarded as a fixed boundary, while the experiment allowed the structure to vibrate. Hence, the lateral expansion of the disks was insignificant and none of the turning of the rectangles was showed. In front of the structure, the computed floe motions were stable and the number of floes flowing out from both sides of the structure were fewer compared to the experiments.

Figure 15 shows the time variation of the x-direction force exerted on the structure. The horizontal axis denotes the elapsed time from the start of floe motion. The results are similar to the circulating water channel experiment. However, the computed highest peaks are about 2 times as high as those of the experiment for both the cases. This difference is due to

the increase of floes colliding with the structure because of the less lateral expansion of disks or the disregarded rotation of rectangles.

4.3 Drift of physical model floes around water stop structure

In this computation, the ocean structure which stopped both the water and floe was used. The initial conditions of this test are the same as those of the previous computations except for the current distribution. Figure 16 shows the computed initial current distribution at the water surface.

Figure 17 shows the time variation of drift of the disk floes and Figure 18 shows the time variation of the x-direction interaction force, exerted on the structure. These are also similar to the experimental results. The floes decrease their speed and begin to move to the wall direction in front of the structure. Then, the first contact of the floes with the structure, being delayed, the highest peak value of the interaction force on the structure decreases and the number of floes which flow out from both sides increases, compared with the case when the structure stops only the floes. The elapsed time from the start of the drift to the first contact of the floes with the structure is about 24 seconds and the two main collisions occur, and the region of the accumulated floes in front of the structure is hardly formed. These agree with the results of the experiment well. However, the highest peak is much lower compared to the experiment. This difference is due to the size of the computation mesh: the mesh is relatively large compared to the structure. This results in the decrease of the water speed and floe momentum in front of the structure.

5. Simulation of Sea Ice Motion in the Southern Part of the Sea of Okhotsk

The numerical simulation covers the sea area around Hokkaido and includes the southern part of the Sea of Okhotsk, the northern part of the Sea of Japan and a part of the Pacific, as shown in Figure 19.

5.1 Computation conditions

The computation domain is divided into 5041 (71×71) square meshes with the size of 12.5 km. The number of water layers was 5 and the height of each layer was 6 m. Initial value of the concentration and ice thickness of sea ice are estimated from observational data from satellites, airplanes, ships and coastal raiders. Figure 19 shows initial distributions of the ice concentration and thickness on 1st February, 1994. The numerical weather prediction data including sea surface pressure and wind velocity at 10 m height are used. Figure 20

shows the time variation of wind velocity in the computation domain.

5.2 Numerical result

Figure 21 shows the predicted and observed distribution of ice concentrations over 7 days, i.e. 8th February. The higher sea ice concentration region at the north-west side of the Siretoko peninsula is accurately predicted. However, the predicted sea ice area extends more eastward in the sea of Okhotsk and southward in the Japan sea west of Sakhalin than that observed.

6. Summary and Conclusions

In a circulation water channel, the drift tests of physical model floes were performed in order to investigate the characteristics of their motion and interaction with a structure. The results are summarized as follows:

The floe motion depends on the floe shapes. The disk floes expand laterally due to the lateral expansion force. The lateral expansion force increases in front of a structure. Then the disks flow out from both sides of the structure and the number of floes in front of the structure decreases with time. However, the rectangle floes scarcely expand laterally. Then the number of floes in front of the structure becomes almost constant with respect to time.

The floe motion also depends on the structure. When the structure stops both the floes and water, the floes decrease their speed in front of the structure and the interaction force on the structure decreases, compared with the case when the structure stops only the floes.

Some computations using the Distributed Mass / Discrete Floe model were made. Simulation results were compared with the circulating water channel experiments and the sea ice motion in the southern part of the Okhotsk. The DMDF predicted the results of the circulating water channel drift tests quite closely. The DMDF results also compared quite well with the sea ice motion.

Acknowledgment

The authors thank Messrs. Kamihira and Toyota, the Japan Meteorological Agency for their cooperation supplying the observation data of the Sea of Okhotsk.

t = 5 seconds

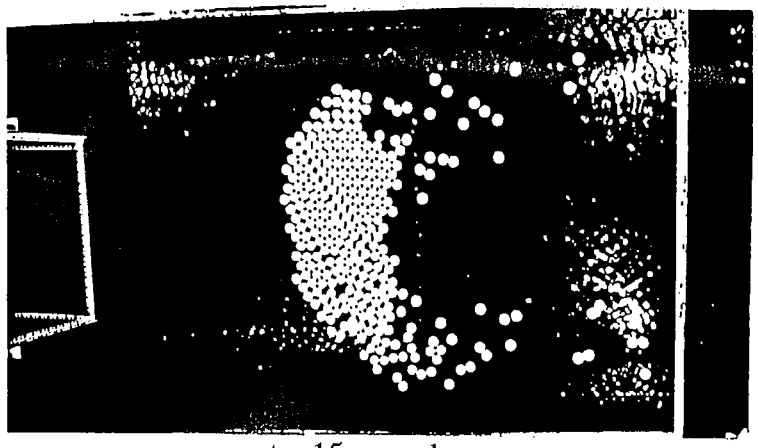

t = 15 seconds

t = 10 seconds

t = 20 seconds

Fig. 5 Free drift of disk floe models

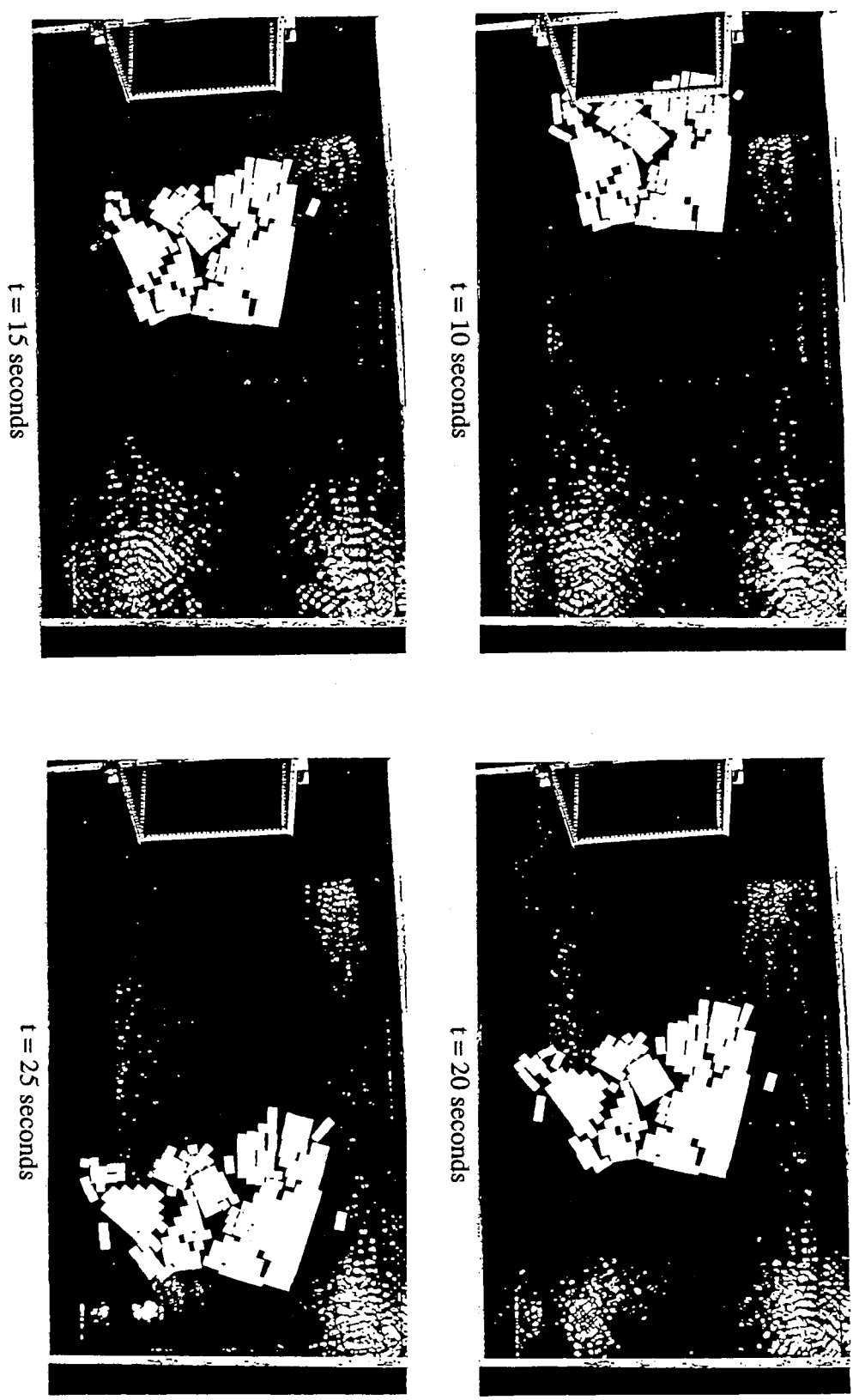

Fig. 6 Free drift of rectangle floe models

t = 10 seconds

t = 20 seconds

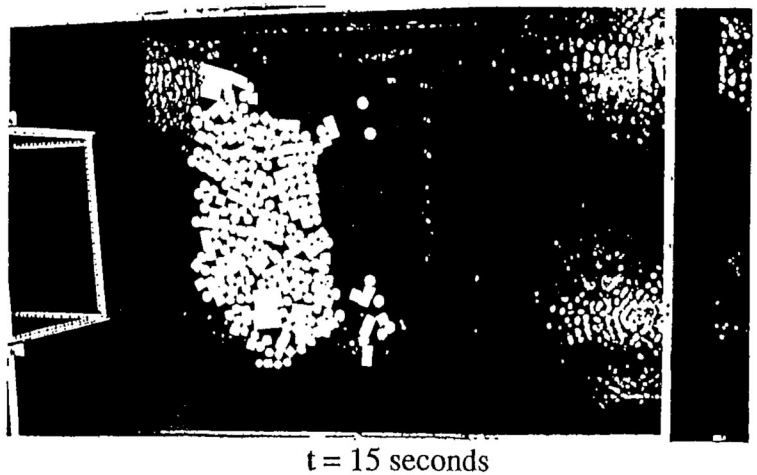

t = 15 seconds

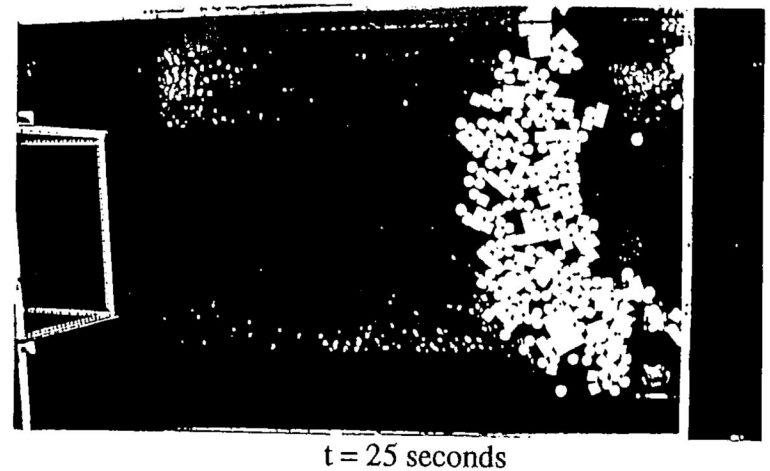

t = 25 seconds

Fig. 7 Free drift of mixture of disk and rectangle floe models

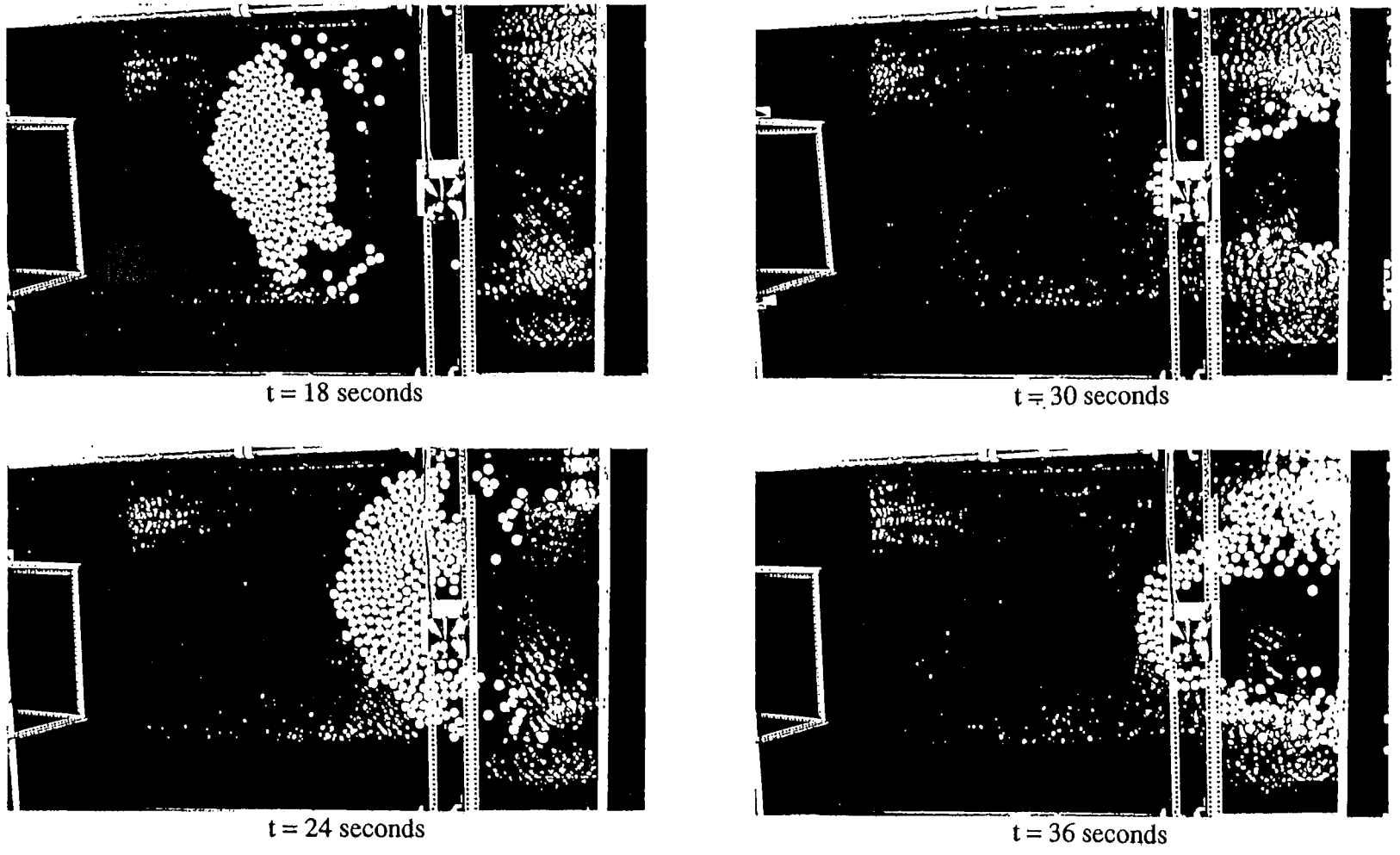

Fig. 8 Drift of disk floe models around the no water stop structure

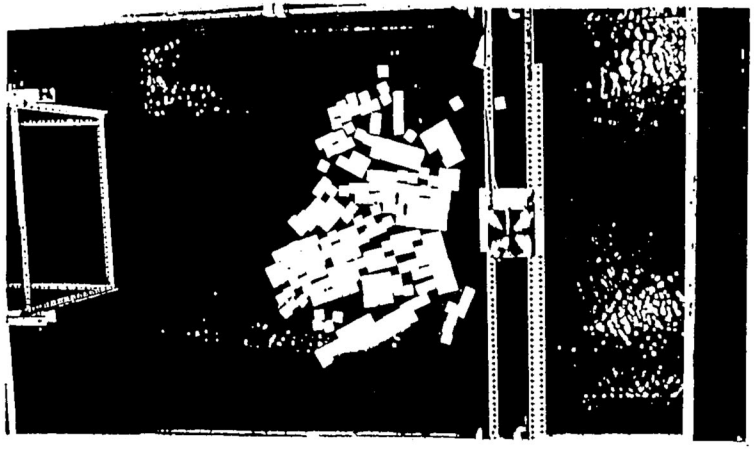

t = 18 seconds

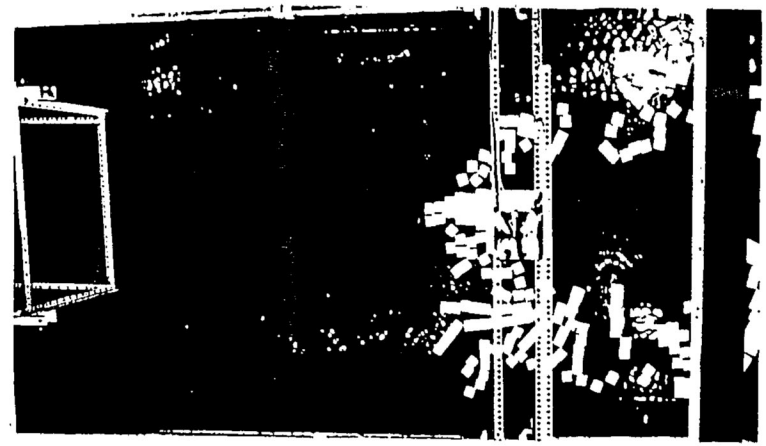

t = 30 seconds

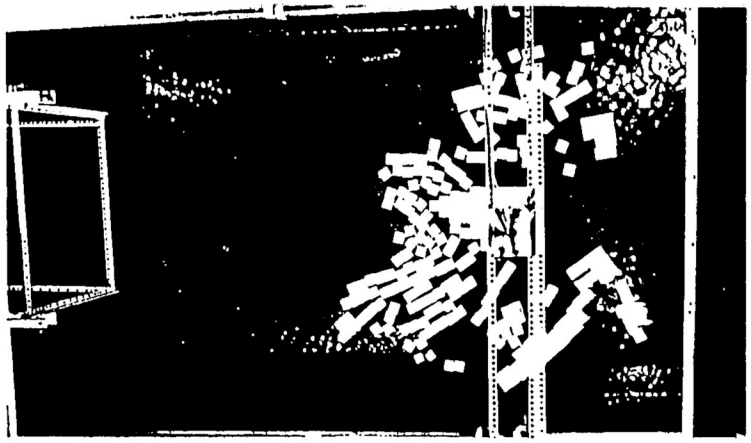

t = 24 seconds

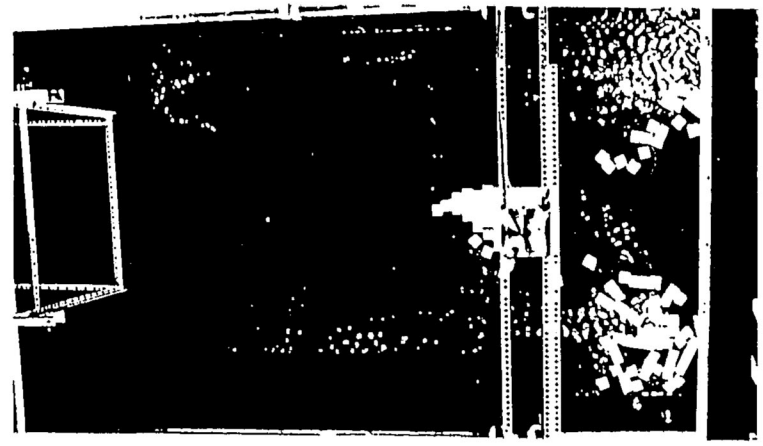

t = 36 seconds

Fig. 9 Drift of rectangle floe models around the no water stop structure

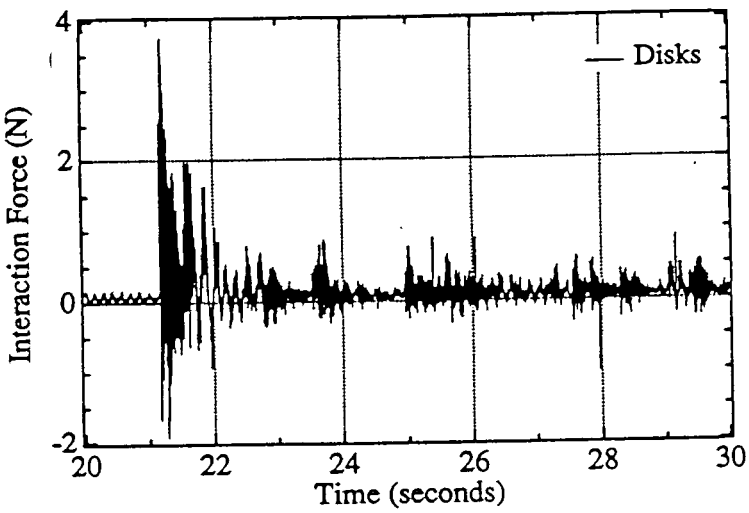

(a) Disk floe models

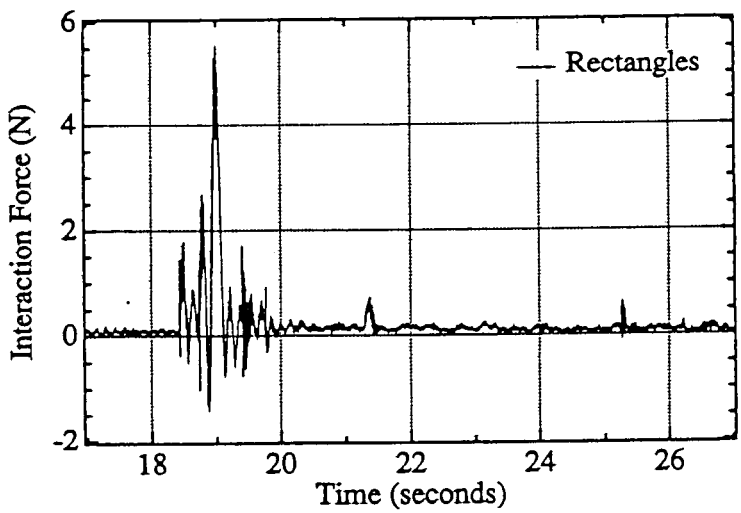

(b) Rectangle floe models

Fig. 10 Measured interaction force on the no water stop structure

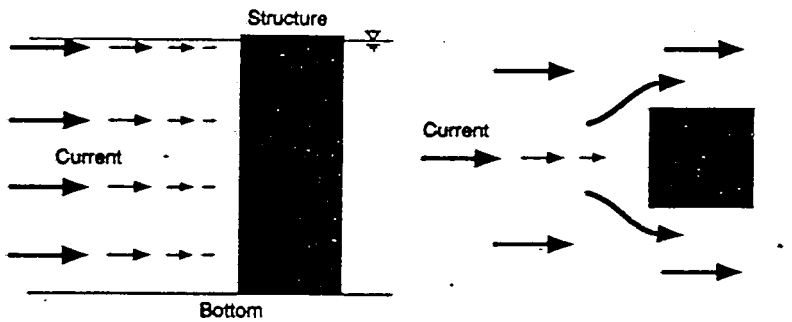

(a) Side View (b) Top View

Fig. 11 Current distribution around the water stop structure

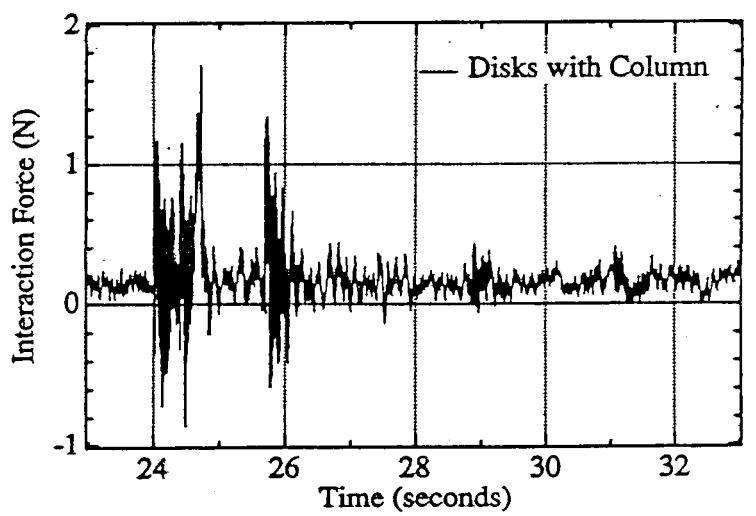

Fig. 13 Measured interaction force on the water stop structure

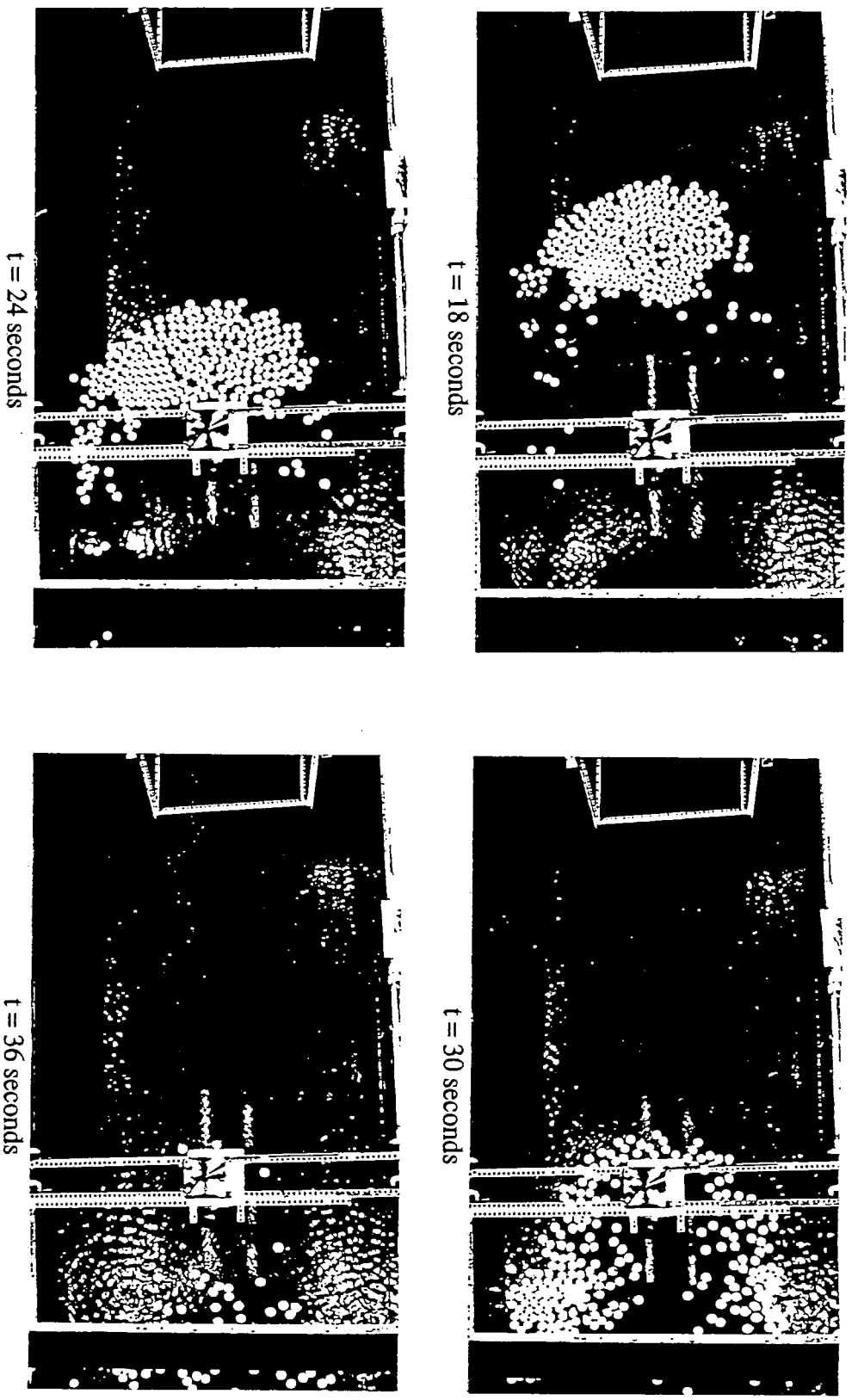

Fig. 12 Drift of disk floe models around the water stop structure

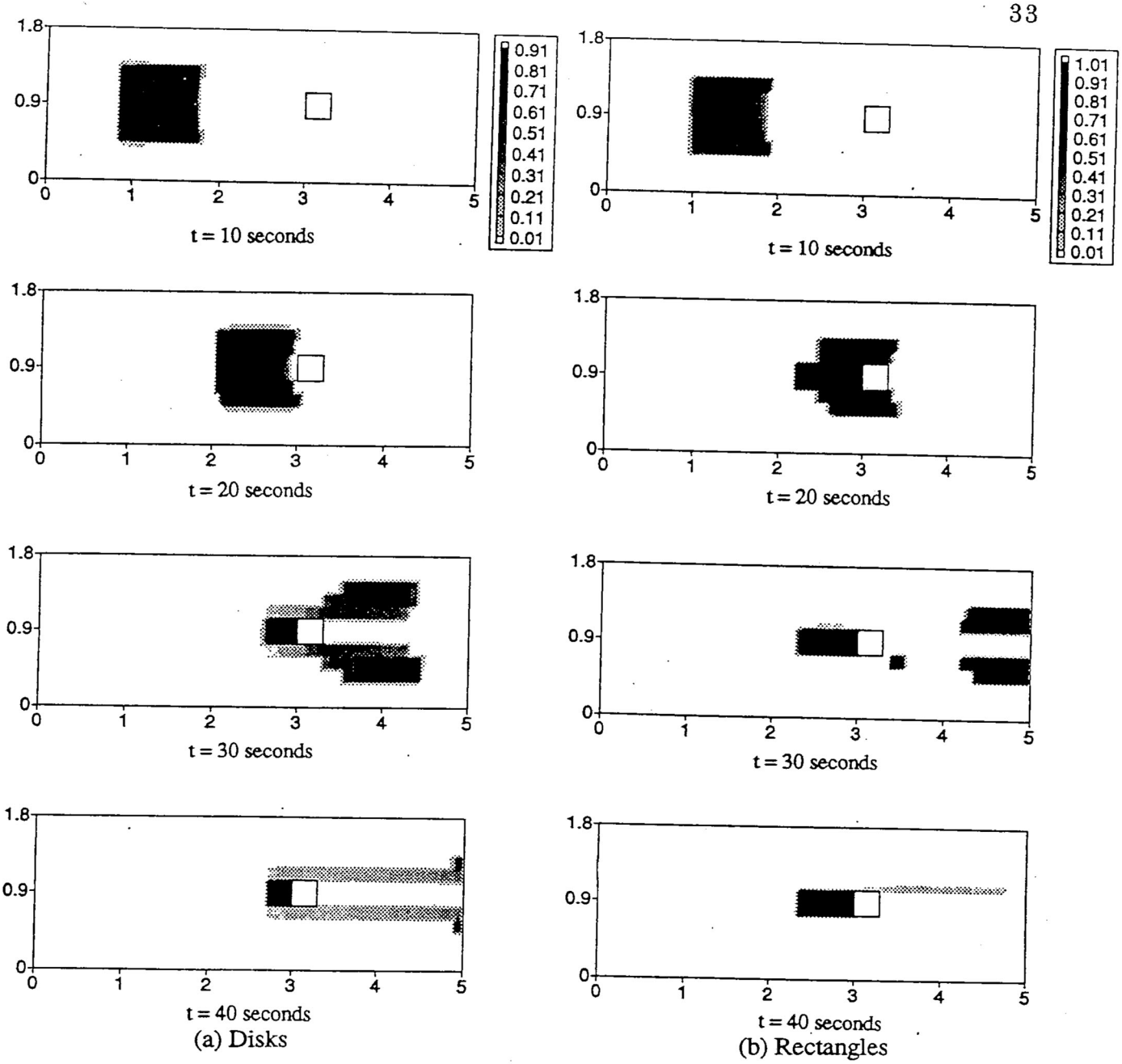

Fig. 14 Computed drift of floes around the no water stop ocean structure

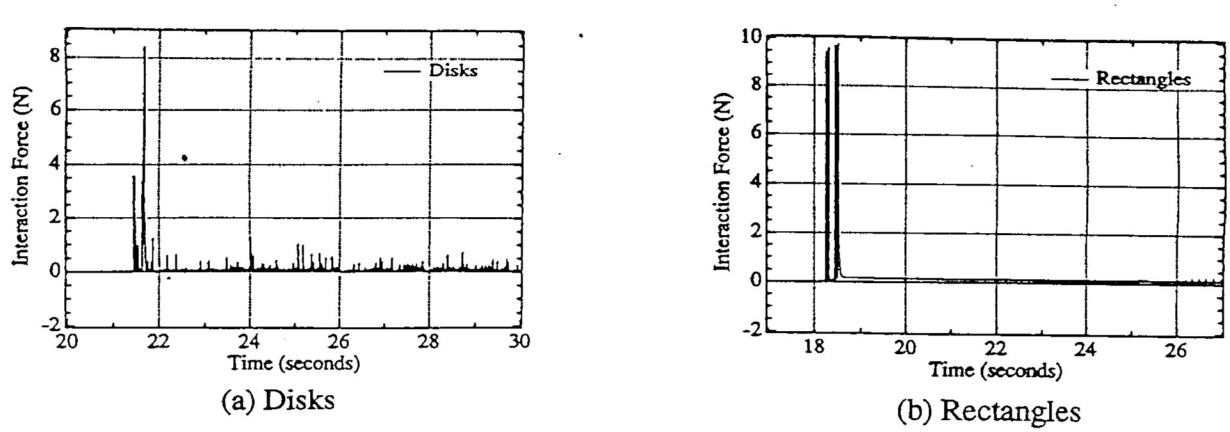

Fig. 15 Computed interaction force on the no water stop ocean structure

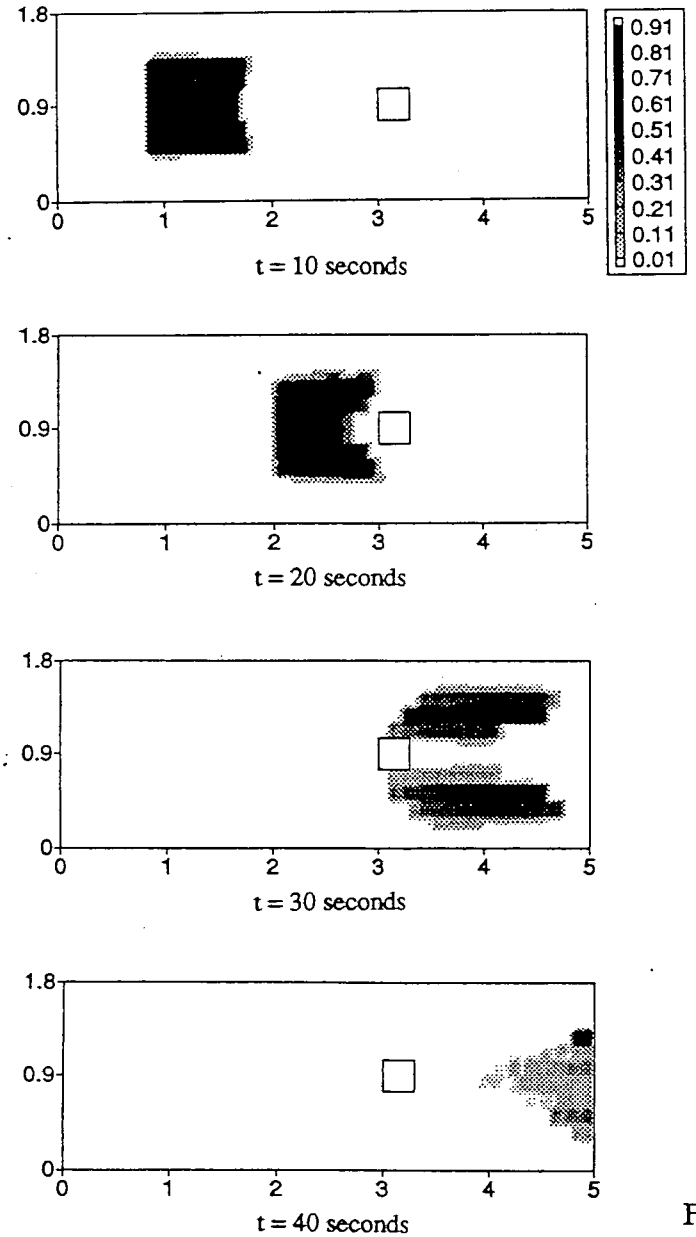

Fig. 17 Computed drift of floes around the water stop ocean structure

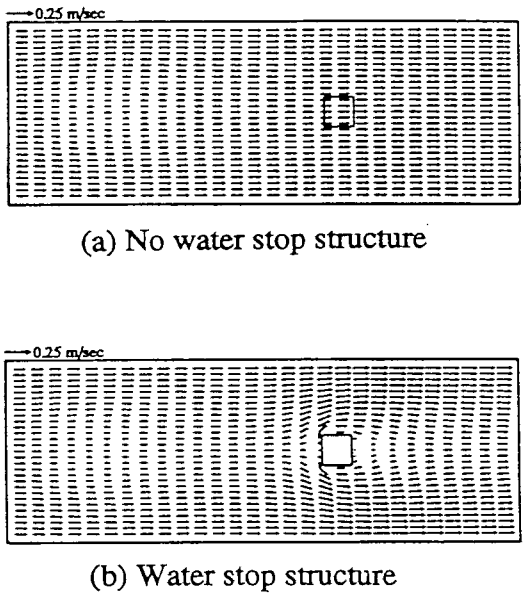

Fig. 16 Current distribution at water surface; the case of mesh size of 6 cm × 6 cm

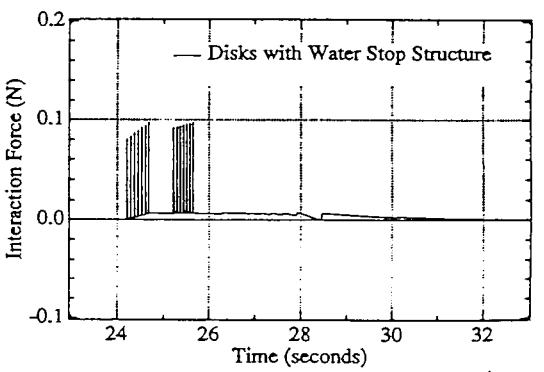

Fig. 18 Computed interaction force on the water stop ocean structure

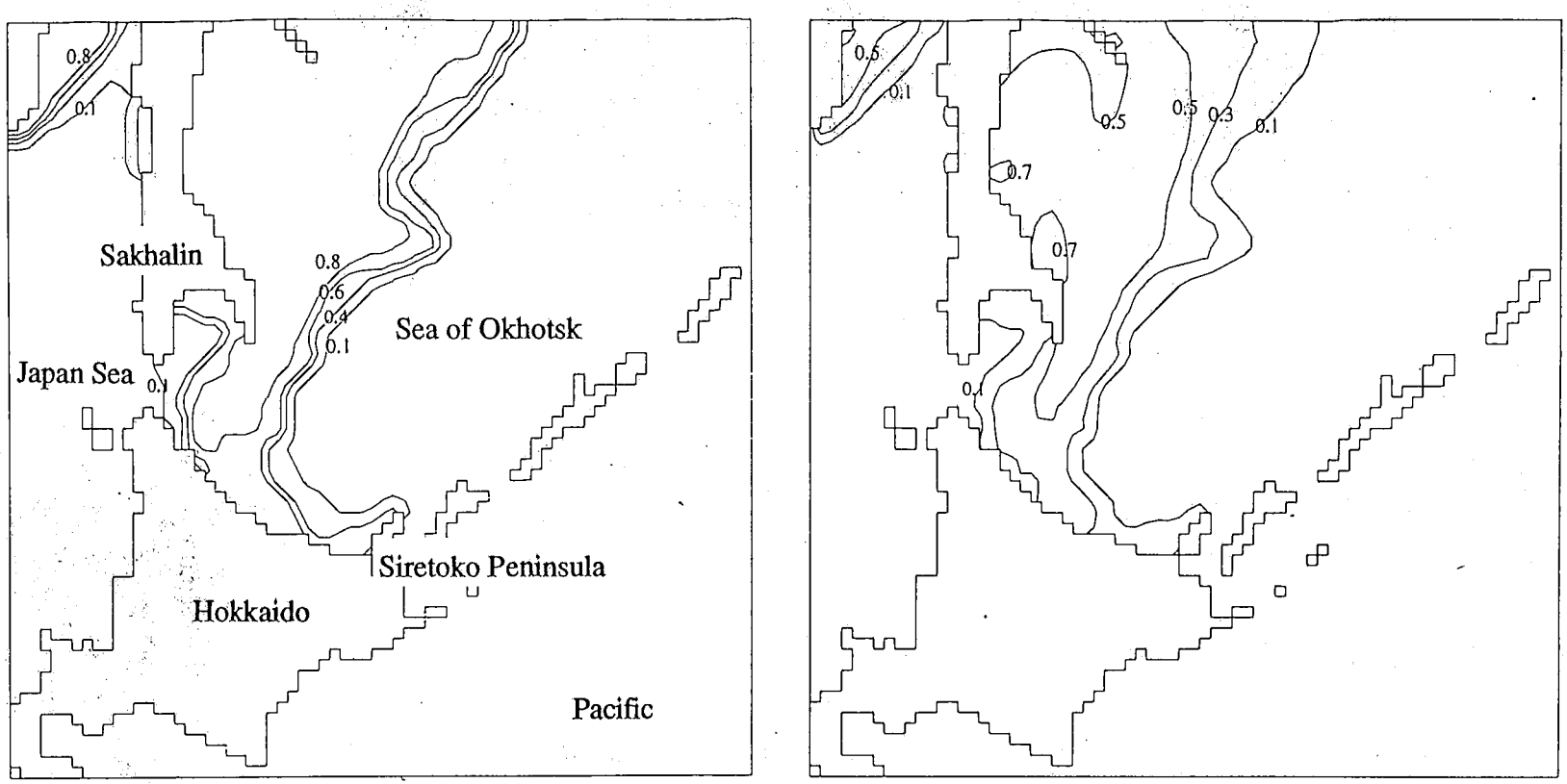

(a) Ice concentration

(b) Ice thickness

Fig. 19 Initial condition of Sea Ice

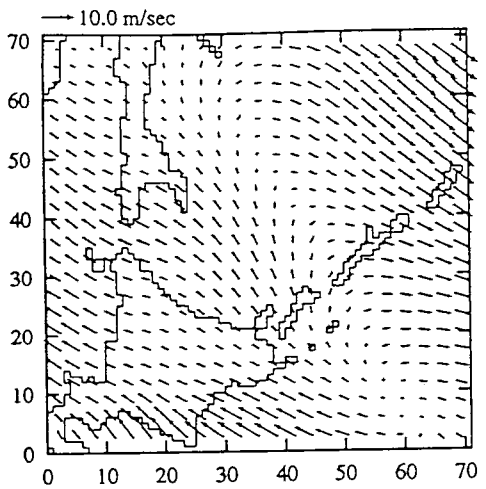

(a) 1 February 1994

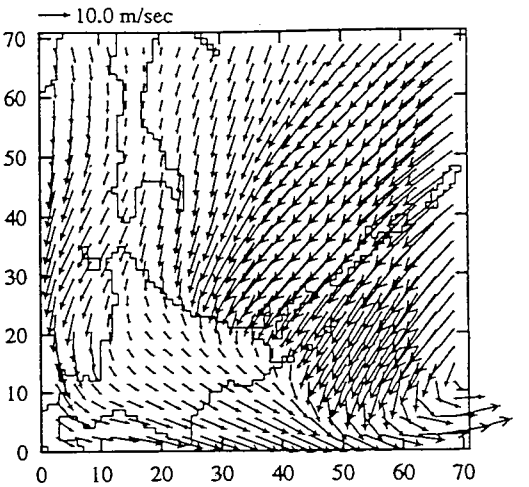

(b) 2 February 1994

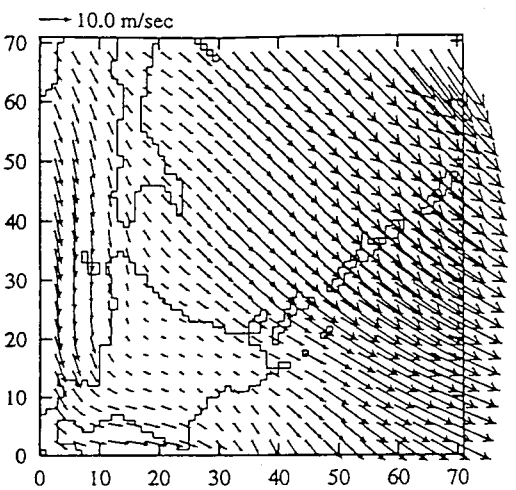

(c) 3 February 1994

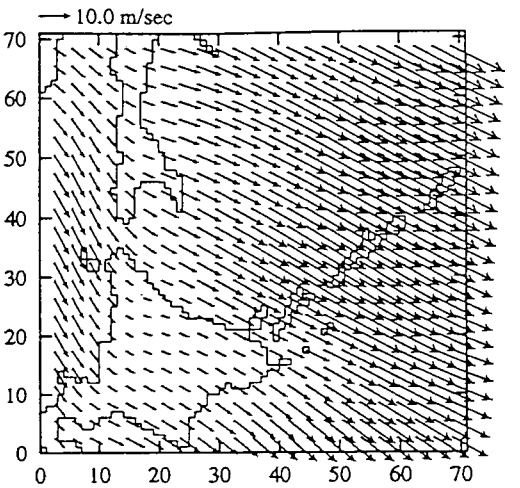

(d) 4 February 1994

Fig. 20 Wind velocity

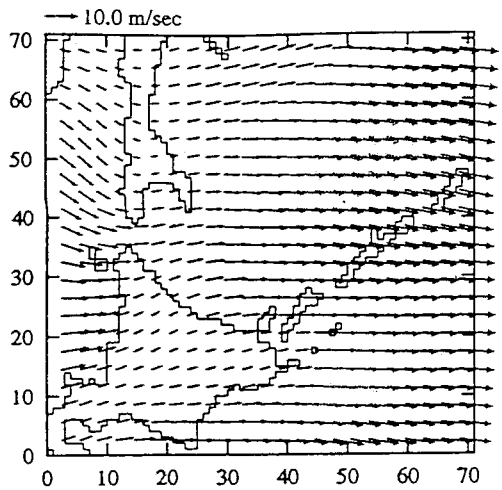

(e) 5 February 1994

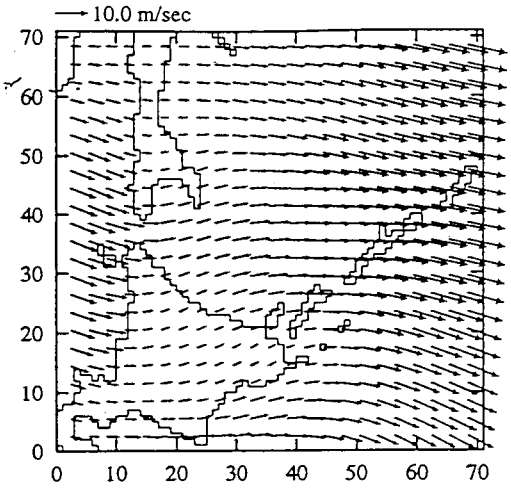

(f) 6 February 1994

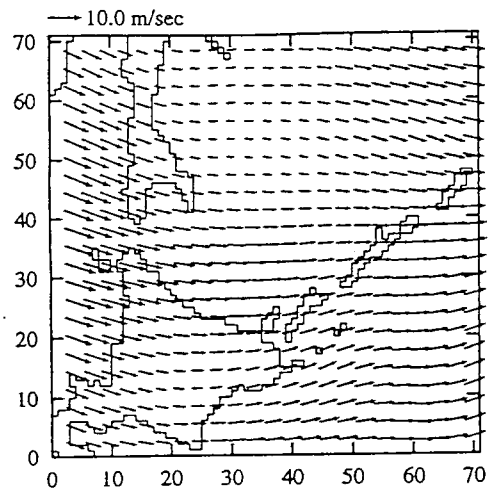

(g) 7 February 1994

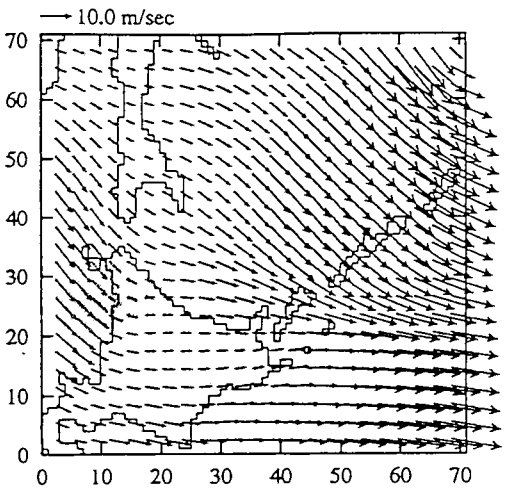

(h) 8 February 1994

Fig. 20 Wind velocity

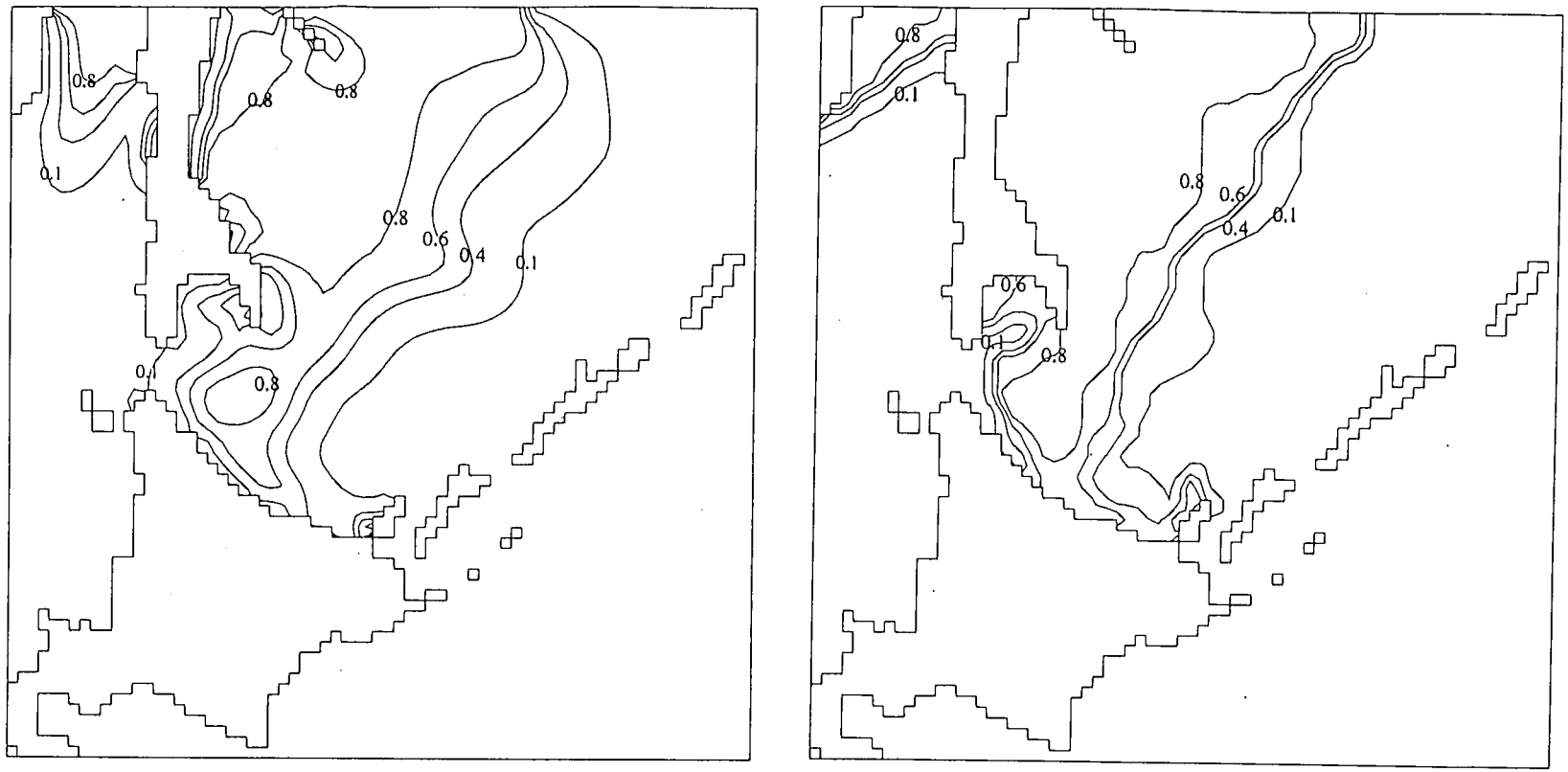

(a) Predicted

(b) Observed

Fig. 21 Ice distribution on 8 February 1994

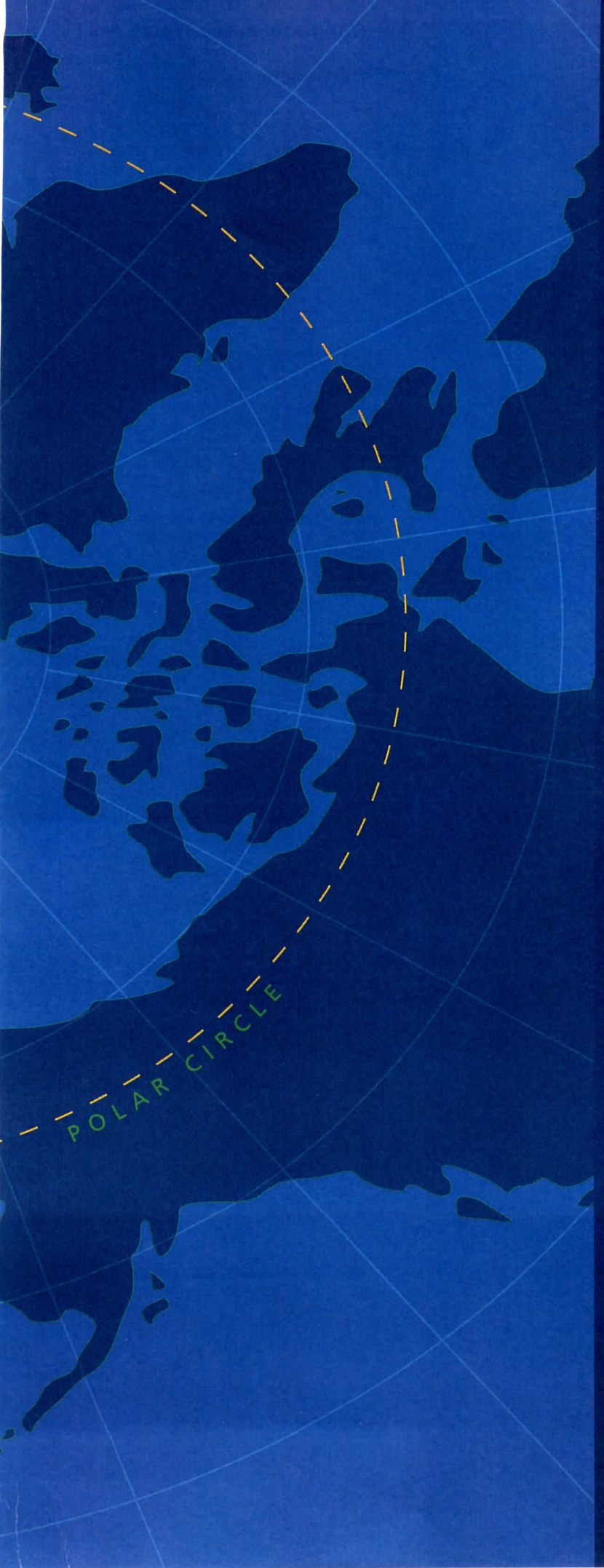

The three main cooperating institutions of INSROP

Ship & Ocean Foundation (SOF), Tokyo, Japan.

SOF was established in 1975 as a non-profit organization to advance modernization and rationalization of Japan's shipbuilding and related industries, and to give assistance to non-profit organizations associated with these industries. SOF is provided with operation funds by the Sasakawa Foundation, the world's largest foundation operated with revenue from motorboat racing. An integral part of SOF, the Tsukuba Institute, carries out experimental research into ocean environment protection and ocean development.

Central Marine Research & Design Institute (CNIIMF), St. Petersburg, Russia.

CNIIMF was founded in 1929. The institute's research focus is applied and technological with four main goals: the improvment of merchant fleet efficiency; shipping safety; technical development of the merchant fleet; and design support for future fleet development. CNIIMF was a Russian state institution up to 1993, when it was converted into a stock-holding company.

The Fridtjof Nansen Institute (FNI), Lysaker, Norway.

FNI was founded in 1958 *and is based at* Polhøgda, the home of Fridtjof Nansen, famous Norwegian polar explorer, scientist, humanist and statesman. The institute spesializes in applied social science research, with special focus on international resource and environmental management. In addition to INSROP, the research is organized in six integrated programmes. Typical of FNI research is a multi-disciplinary approach, entailing extensive cooperation with other research institutions both at home and abroad. The INSROP Secretariat is located at FNI.